nature medicine

MST1 is a key regulator of beta cell apoptosis and dysfunction in diabetes

Amin Ardestani[1], Federico Paroni[1,6], Zahra Azizi[1,6], Supreet Kaur[1,6], Vrushali Khobragade[1], Ting Yuan[1], Thomas Frogne[2], Wufan Tao[3], Jose Oberholzer[4], Francois Pattou[5], Julie Kerr Conte[5] & Kathrin Maedler[1]

Apoptotic cell death is a hallmark of the loss of insulin-producing beta cells in all forms of diabetes mellitus. Current treatments fail to halt the decline in functional beta cell mass, and strategies to prevent beta cell apoptosis and dysfunction are urgently needed. Here, we identified mammalian sterile 20–like kinase-1 (MST1) as a critical regulator of apoptotic beta cell death and function. Under diabetogenic conditions, MST1 was strongly activated in beta cells in human and mouse islets and specifically induced the mitochondrial-dependent pathway of apoptosis through upregulation of the BCL-2 homology-3 (BH3)-only protein BIM. MST1 directly phosphorylated the beta cell transcription factor PDX1 at T11, resulting in the latter's ubiquitination and degradation and thus in impaired insulin secretion. MST1 deficiency completely restored normoglycemia, beta cell function and survival *in vitro* and *in vivo*. We show MST1 as a proapoptotic kinase and key mediator of apoptotic signaling and beta cell dysfunction and suggest that it may serve as target for the development of new therapies for diabetes.

Pancreatic beta cell death is the fundamental cause of type 1 diabetes (T1D) and a contributing factor to the reduced beta cell mass in type 2 diabetes (T2D)[1–4]. In both cases, the mechanisms of beta cell death are complex and as yet not fully defined. Thus, multiple triggering factors have been identified; these factors initiate a variety of signaling cascades that affect the expression of apoptotic genes, leading to subsequent beta cell failure. In T1D, autoimmune destruction of insulin-producing beta cells and critically diminished beta cell mass are hallmarks of the disease[2]. Beta cell destruction occurs through immune-mediated processes; mononuclear cell infiltration in the pancreatic islets and interaction between antigen-presenting cells and T cells lead to high local concentrations of inflammatory cytokines, chemokines, reactive oxygen species and other apoptotic triggers (for example, the perforin and Fas–Fas ligand systems)[2]. In T2D, beta cell dysfunction and reduced beta cell mass are the ultimate events leading to the development of clinically overt disease in insulin-resistant individuals. Beta cell destruction is caused by multiple stimuli including glucotoxicity, lipotoxicity, proinflammatory cytokines, endoplasmic reticulum stress and oxidative stress[5]. Unfortunately, although it has been demonstrated that even a small amount of preserved endogenous insulin secretion has great benefits in terms of clinical outcome[6], none of the currently widely used antidiabetic agents target the maintenance of endogenous beta cell mass.

Beta cells are highly sensitive to apoptotic damages induced by multiple stressors such as inflammatory and oxidative assault, owing at least in part to their low expression of cytoprotective enzymes[7]. The initial trigger of beta cell death still remains unclear; it follows an orchestra of events, which makes the initiation of beta cell death complex and its blockade difficult to successfully achieve *in vivo*. Therefore, the identification of a common key regulator of beta cell apoptosis would offer a new therapeutic target for the treatment of diabetes.

The identification of the genes that regulate apoptosis has laid the foundation for the discovery of new drug targets. MST1 (also known as STK4 and KRS2) is a ubiquitously expressed serine-threonine kinase that is part of the Hippo signaling pathway and involved in multiple cellular processes such as morphogenesis, proliferation, stress response and apoptosis[8,9]. MST1 is a target and activator of caspases, serving to amplify the apoptotic signaling pathway[10,11]. Thr183 in subdomain VIII of MST1 has been defined as a primary site for the phosphoactivation and the autophosphorylation of MST1 and is essential for kinase activation. Both phosphorylation and caspase-mediated cleavage are required for full activation of MST1 during apoptosis. MST1 promotes cell death through regulation of multiple downstream targets such as LATS1 and LATS2, histone H2B and members of the FOXO family, as well as through induction of stress kinase c-Jun-N-terminal kinase (JNK) and activation of caspase-3 (refs. 9,12,13).

Genetic mutations and/or metabolic disturbances can alter protein networks and thereby disrupt downstream signaling pathways that are essential for beta cell survival and function. The transcription factor pancreatic duodenal homeobox-1 (PDX1, previously called IPF1, IDX1, STF1 or IUF1)[14,15] is a key mediator of beta cell development and function[16]. In humans, mutations in the *PDX1* gene can predispose individuals to develop maturity onset diabetes of the young, type 4 (MODY 4)[17], suggesting a critical role for PDX1 in

[1]Centre for Biomolecular Interactions Bremen, University of Bremen, Bremen, Germany. [2]Department of Incretin & Islet Biology, Novo Nordisk A/S, Denmark. [3]State Key Laboratory of Genetic Engineering and National Center for International Research of Development and Disease, Institute of Developmental Biology and Molecular Medicine, Fudan University, Shanghai, China. [4]Division of Transplantation, University of Illinois at Chicago, Chicago, Illinois, USA. [5]INSERM U859 Biotherapies for Diabetes, European Genomic Institute for Diabetes, Lille Regional Hospital Center, University of Lille, Lille, France. [6]These authors contributed equally to this work. Correspondence should be addressed to K.M. (kmaedler@uni-bremen.de) or A.A. (ardestani.amin@gmail.com).

Received 5 December 2013; accepted 21 January 2014; published online 16 March 2014; doi:10.1038/nm.3482

mature beta cells; reduced PDX1 expression affects insulin production and secretion and predisposes to beta cell apoptosis[16,18].

Because MST1 acts as common mediator in multiple apoptotic signaling pathways, we hypothesized that it is an initiating trigger of apoptotic signaling in beta cells. MST1 depletion completely restored normoglycemia and insulin secretion and prevented diabetes progression. These findings suggest that MST1 could be a fundamental target for diabetes therapy.

RESULTS

MST1 is activated in diabetes

To test whether MST1 activation is correlated with beta cell apoptosis, we exposed isolated human and mouse islets and the rat beta cell line INS-1E to a complex diabetogenic milieu. MST1 activity was highly upregulated in these cells under these conditions (created through incubation with the cytokines interleukin-1β (IL-1β) and interferon-γ (IFN-γ) (IL/IF), upon chronic exposure to increasing glucose concentrations (22.2 and 33.3 mM) or palmitic acid, or upon exposure to acute oxidative stress from hydrogen peroxide) (**Fig. 1a–c** and **Supplementary Fig. 1a**,**b**). The upregulation of MST1 occurred by both caspase-mediated cleavage and autophosphorylation (yielding MST1 phosphorylated on T183 (pMST1)). This was accompanied by higher phosphorylation of histone H2B as well as induction of JNK signaling (**Fig. 1a–c**). In contrast, short-term culture with high glucose concentrations (11.2, 22.2 and 33.3 mM) induced neither apoptosis nor MST1 cleavage and phosphorylation (**Supplementary Fig. 1d**). MST1 was also activated in islets from subjects with T2D (**Fig. 1d**), obese diabetic *Lepr*^{db} mice (*db/db* mice, **Fig. 1e**) and hyperglycemic mice fed with a high-fat, high-sucrose diet (HFD) for 16 weeks (**Supplementary Fig. 1c**). This activation correlated directly with beta cell apoptosis as described previously[19], as whenever MSTI was induced, apoptosis was also higher. To confirm the beta cell–specific upregulation of MST1, we performed double immunostaining for pMST1 and insulin in pancreatic islets from subjects with poorly controlled T2D (**Fig. 1d**) and pancreatic islets from *db/db* mice (**Fig. 1e**) and found pMST1 staining in beta cells, whereas there was almost no signal in cells from subjects without diabetes or control mice.

Caspase-3 and JNK act not only as downstream targets but also as upstream activators of MST1 through cleavage- and phosphorylation-dependent mechanisms[12,20], and they may initiate a vicious cycle and a proapoptotic signaling cascade in beta cells. Using inhibitors of JNK (SP600125) and caspase-3 (z-DEVD-fmk) and siRNA to caspase-3, we found that both JNK and caspase-3 were responsible for stress-induced MST1 cleavage by diabetic stimuli in human islets and INS-1E cells (**Supplementary Fig. 1e–h**), suggesting that MST1 induces a positive feedback loop with caspase-3 under diabetogenic conditions.

Because phosphatidylinositol-3 kinase (PI3K)-AKT signaling is a key regulator of beta cell survival and function[21,22] and MST1 signaling is negatively regulated by this pathway in other cell types[23,24], we hypothesized that AKT is an important negative regulator of MST1. Maintaining AKT activation through either exogenous addition of mitogens such as glucagon-like peptide-1 (GLP1) or insulin or overexpression of constitutively active AKT1 (Myr-AKT1, containing a myristoylation sequence and HA tag) inhibited glucose- and cytokine-induced phosphorylation of MST1, MST1 cleavage and apoptosis (**Fig. 1f** and **Supplementary Fig. 2a–d**). As GLP1 and insulin exert their cell survival actions primarily through the PI3K-AKT pathway[21,25], we tested whether inhibition of this pro-survival signaling might enhance MST1 activation. PI3K and AKT were inhibited by LY294002, and triciribine (an AKT inhibitor) led to lower levels of phosphorylation of Gsk3 and Foxo1, two well-characterized AKT substrates, and induced MST1 activation (**Fig. 1g**,**h** and **Supplementary Fig. 2e**). We further corroborated these findings using siRNA against AKT, which led to a critical upregulation of MST1 activity and potentiated cytokine-induced phosphorylation of MST1 and beta cell death (**Supplementary Fig. 2f**). MST1 overexpression also diminished insulin-induced AKT phosphorylation and, conversely, there was higher AKT phosphorylation in MST1-depleted beta cells (**Fig. 1i**). Knockdown of MST1 expression antagonized the apoptotic effect of AKT inactivation in INS-1E cells, implicating endogenous MST1 in the apoptotic mechanism induced by PI3K-AKT inhibition (**Supplementary Fig. 2g**,**h**). In summary, these results suggest that MST1 is activated in prodiabetic conditions *in vitro* and *in vivo*, antagonized by PI3K-AKT signaling and dependent on the JNK- and caspase-induced apoptotic machinery.

MST1 induces beta cell death

MST1 overexpression alone was also sufficient to induce apoptosis in human and rat beta cells (**Fig. 2a–c**). To investigate pathways that potentially contribute to MST1-induced beta cell apoptosis, we overexpressed MST1 in human islets and rat INS-1E cells through an adenoviral system, which efficiently upregulated MST1, activated JNK and induced beta cell apoptosis, as determined by an increased number of TUNEL-positive beta cells as well as caspase-3 activation and cleavage of poly-(ADP-ribose) polymerase (PARP), a downstream substrate of caspase-3 (**Fig. 2a–c**). Previous data proposed a role for the mitochondrial pathway in MST-dependent signaling[26,27]. Evaluation of established mitochondrial proteins in MST1-overexpressing islets and INS-1E cells showed cleavage of the initiator caspase-9, release of cytochrome *c*, induction of proapoptotic BAX and a decline in antiapoptotic BCL-2 and BCL-xL levels (**Fig. 2b**,**c** and **Supplementary Fig. 3a**), which led to a reduction of BCL-2/BAX and BCL-xL/BAX ratios. Notably, MST1-induced caspase-3 cleavage was reduced by treatment of human islets with the Bax inhibitor peptide V5 (**Fig. 2d**), which has been shown to promote beta cell survival[28]; together, these findings emphasize that MST1-induced apoptosis proceeds via the mitochondrial-dependent pathway. We also analyzed the expression of BH3-only proteins as regulators of the intrinsic cell death pathway[29]. Of these, BIM was robustly induced, whereas other BH3-only protein levels remained unchanged (**Fig. 2b**,**c** and **Supplementary Fig. 3b**). To assess whether kinase activity of MST1 is required for altering mitochondrial-dependent proteins and induction of apoptosis, we overexpressed a kinase-dead mutant of MST1 (K59R; dominant-negative MST1 (ref. 30)) in human islets. Unlike wild-type (WT) MST1, MST1-K59R did not change the levels of BIM, BAX, BCL-2, BCL-xL and caspase-3 cleavage (**Supplementary Fig. 3c**). We next determined whether BIM is a major molecule whose action would override the proapoptotic action of MST1. Indeed, BIM depletion led to a significant reduction of MST1-induced apoptosis in human islets (**Fig. 2e**,**f**).

Overexpression of MST1 further potentiated glucose-induced apoptosis in beta cells in a BIM-dependent manner (**Supplementary Fig. 3d**). BIM is regulated by the JNK[31] and AKT[32] signaling pathways. MST1-induced increase in BIM and subsequent caspase-3 cleavage was prevented by JNK inhibition through overexpression of dn-JNK1 (**Fig. 2g**) or by the JNK inhibitor (**Supplementary Fig. 3e**), which suggests that MST1 uses JNK signaling to mediate BIM upregulation and induction of apoptosis. We confirmed the involvement of AKT in the regulation of MST1-induced apoptosis by overexpressing

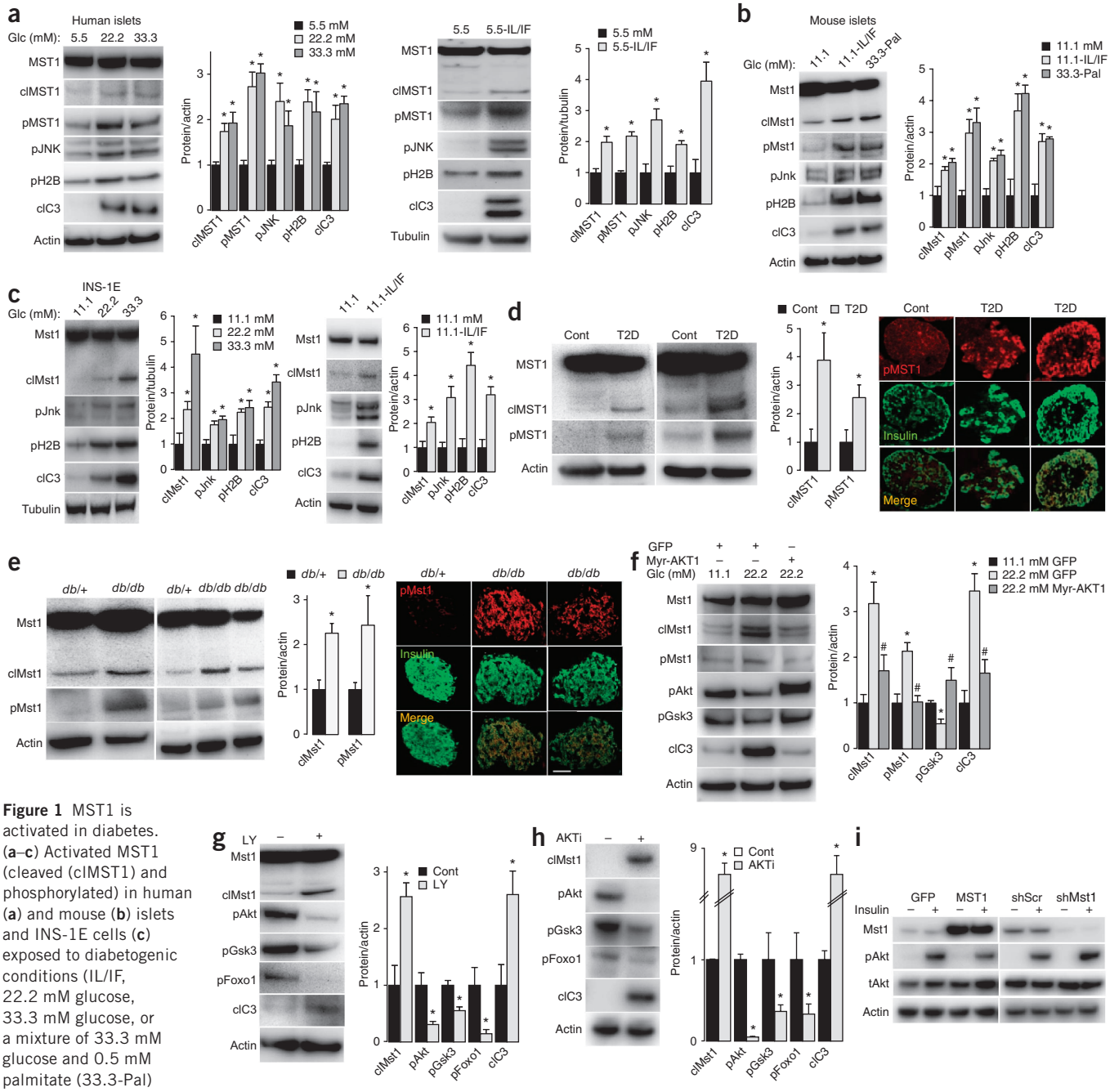

Figure 1 MST1 is activated in diabetes. (**a**–**c**) Activated MST1 (cleaved (cIMST1) and phosphorylated) in human (**a**) and mouse (**b**) islets and INS-1E cells (**c**) exposed to diabetogenic conditions (IL/IF, 22.2 mM glucose, 33.3 mM glucose, or a mixture of 33.3 mM glucose and 0.5 mM palmitate (33.3-Pal) for 72 h). Western blots of MST1, pMST1, pJNK, pH2B and caspase-3 cleavage (cIC3) and densitometry analyses are shown. Cont, control; Glc, glucose. (**d**,**e**) Activated MST1 in islets. Human isolated islets from nondiabetic control subjects ($n = 7$) and subjects with T2D ($n = 4$, all with documented fasting plasma glucose >150 mg/dl) (**d**) and from 10-week-old diabetic *db/db* mice ($n = 5$) and their heterozygous littermates (*db/+*, $n = 5$) (**e**). Left, western blots of MST1 and pMST1 and densitometry analyses. Right, double immunostaining for pMST1 (red) and insulin (green) in sections from human isolated islets from nondiabetic control subjects and subjects with T2D and from 6-week-old diabetic *db/db* mice (representative analyses from 10 pancreases from subjects with T2D and >10 pancreases from control subjects and from 7 *db/db* mice and 7 heterozygous controls are shown). Scale bar, 100 μm. (**f**) Western blots of Mst1, clMst1, pMst1, pAkt, pGsk3 and caspase-3 cleavage and densitometry analysis for INS-1E cells transfected with GFP control or Myr-AKT1 expression plasmids exposed to 22.2 mM glucose for 72 h. (**g**) Western blots of Mst1, clMst1, pAkt, pGsk3, pFoxo1 and caspase-3 cleavage and densitometry analysis for INS-1E cells exposed to the PI3K inhibitor LY294002 (LY, 10 μM for 8 h). (**h**) Western blots of clMst1, pAkt, pGsk3, pFoxo1 and caspase-3 cleavage and densitometry analysis for INS-1E cells exposed to the AKT inhibitor triciribine (AKTi, 10 μM for 6 h). (**i**) Western blots of Mst1, pAkt and tAkt for INS-1E cells infected with an adenovirus expressing GFP (Ad-GFP) or MST1 (Ad-MST1) or transfected with shMst1 or shScr control expression plasmids for 48 h, serum-starved for 12 h and then stimulated with insulin. All graphs show densitometry analyses from at least 3 independent experiments normalized to actin or tubulin. All western blots show representative results from at least 3 independent experiments from 3 different donors or mice. Tubulin or actin was used as loading control. Data are expressed as means ± s.e.m. $^{*}P < 0.05$ compared to untreated or nondiabetic control. $^{\#}P < 0.05$ Myr-AKT1 compared to GFP at 22.2 mM glucose.

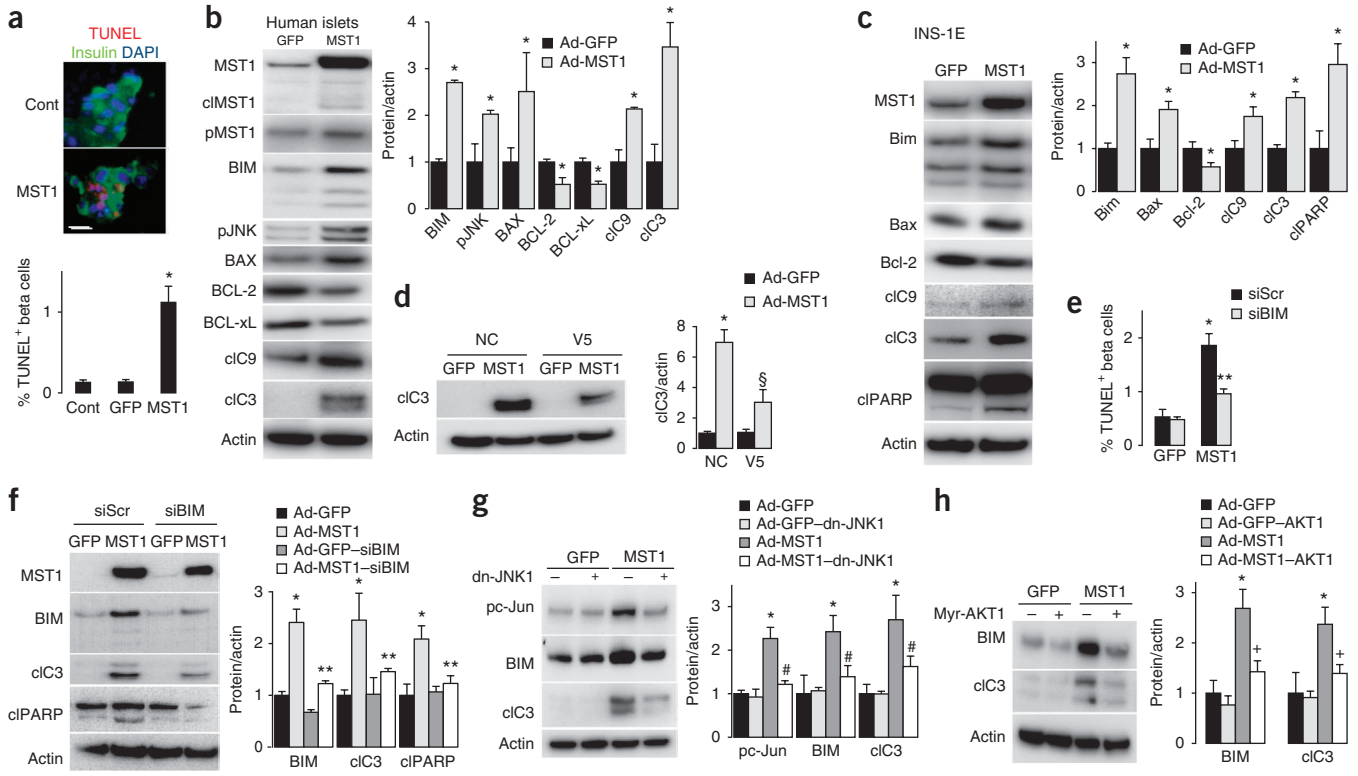

Figure 2 MST1 induces beta cell death. (**a**–**d**) MST1 overexpression in human islets (**a**,**b**) and INS-1E cells (**c**) for 48 h. Triple staining for DAPI (blue), TUNEL (red) and insulin (green) (**a**) TUNEL analysis from an average number of 18,501 insulin-positive beta cells. Scale bar, 100 µm. (**b**,**c**) Adenovirus-mediated upregulation of MST1. Western blots and densitometry analysis of MST1, cleaved MST1, BIM, pJNK, BAX, BCL-2, BCL-xL, cleaved caspase-9 (cIC9), cleaved caspase-3 and PARP in human islets (**b**) and INS-1E cells (**c**). (**d**) Western blot and densitometry analysis of caspase-3 cleavage from Ad-GFP– or Ad-MST1–infected human islets exposed to BAX inhibitory peptide V5 or negative control (NC) peptide for 36 h. (**e**,**f**) Human islets transfected with BIM siRNA (siBIM) or control Scr siRNA (siScr) infected with Ad-GFP or Ad-MST1 for 48 h. (**e**) Analysis of cells positive for both TUNEL and insulin out of 10,378 insulin-positive counted beta cells. (**f**) Western blot and densitometry analysis of MST1, BIM and caspase-3 and PARP cleavage. (**g**) Western blot and densitometry analysis of pc-Jun, BIM and caspase-3 cleavage from human islets transfected with GFP or dn-JNK1 expression plasmids and infected with Ad-GFP or Ad-MST1 for 48 h. (**h**) Western blot and densitometry analysis of BIM and caspase-3 cleavage from human islets transfected with GFP or Myr-AKT1 expression plasmids and infected with Ad-GFP or Ad-MST1 for 48 h. All graphs show densitometry analysis from at least 3 independent experiments normalized to actin. All western blots show representative results from at least 3 independent experiments from 3 different donors (human islets). Actin was used as loading control. TUNEL analyses are from 3 independent experiments from 3 different donors. Data are expressed as means ± s.e.m. $^{*}P < 0.05$ MST1 overexpression compared to GFP control, §$P < 0.05$ V5-MST1 compared to MST1, $^{**}P < 0.05$ siBIM-MST1 compared to siScr-MST1, $^{\#}P < 0.05$ dn-JNK–MST1 compared to MST1, $^{+}P < 0.05$ AKT1-MST1 compared to MST1.

both MST1 and Myr-AKT1, which reduced BIM induction and caspase-3 cleavage (**Fig. 2h**), indicating that AKT negatively regulates the downstream target of MST1. These data suggest that MST1 is a critical mediator of beta cell apoptosis through activation of the BIM-dependent intrinsic apoptotic pathway and controlled by AKT and JNK signaling pathways.

MST1 impairs beta cell function by destabilizing PDX1

We hypothesized that MST1 activation may elicit changes in beta cell–specific gene transcription that initiate the process of beta cell failure. Overexpression of MST1 led to a complete loss of glucose-stimulated insulin secretion (GSIS; **Fig. 3a** and **Supplementary Fig. 4a**), which could not be accounted for solely by the induction of apoptosis. Previously, we noted that the critical beta cell transcription factor PDX1, which mediates glucose-induced insulin gene transcription in mature beta cells[16,18], is mislocalized and reduced in diabetes[19]. These changes are subsequently associated with impaired beta cell function and hyperglycemia. Stress-induced kinases such as JNK and glycogen synthase kinase-3 (GSK3) phosphorylate PDX1, antagonizing its activity[33,34], which leads to beta cell failure. Thus, we hypothesized that the drastic reduction in insulin secretion following MST1 overexpression may be mediated by PDX1. PDX1 levels were markedly reduced in response to MST1 overexpression in human islets (**Fig. 3b**) and INS-1E cells (**Supplementary Fig. 4b**). In contrast, MST1 overexpression did not affect the amount of mRNA encoding PDX1 (**Fig. 3b** and **Supplementary Fig. 4b**), suggesting that MST1 may regulate PDX1 at the post-transcriptional level. Analysis of PDX1 target genes demonstrated that overexpression of MST1 significantly downregulated *INS* (*Ins1* or *Ins2* for INS-1E), *SLC2A2* and *GCK* in human islets (**Fig. 3b**) and INS-1E cells (**Supplementary Fig. 4b**). Although SLC2A2 is not the predominant glucose transporter in human beta cells[35], we analyzed its expression to provide comparison to the mouse data.

To gain better insight into the role of MST1 in regulation of insulin secretion, we performed GSIS using two insulin secretagogues: GLP1 and glibenclamide. MST1 overexpression significantly abolished GLP1-enhanced glucose-induced insulin secretion ($P < 0.05$ compared to control condition), whereas glibenclamide-induced insulin secretion was not affected, suggesting that defective insulin secretion may occur at a step upstream of calcium influx (**Supplementary Fig. 4c**).

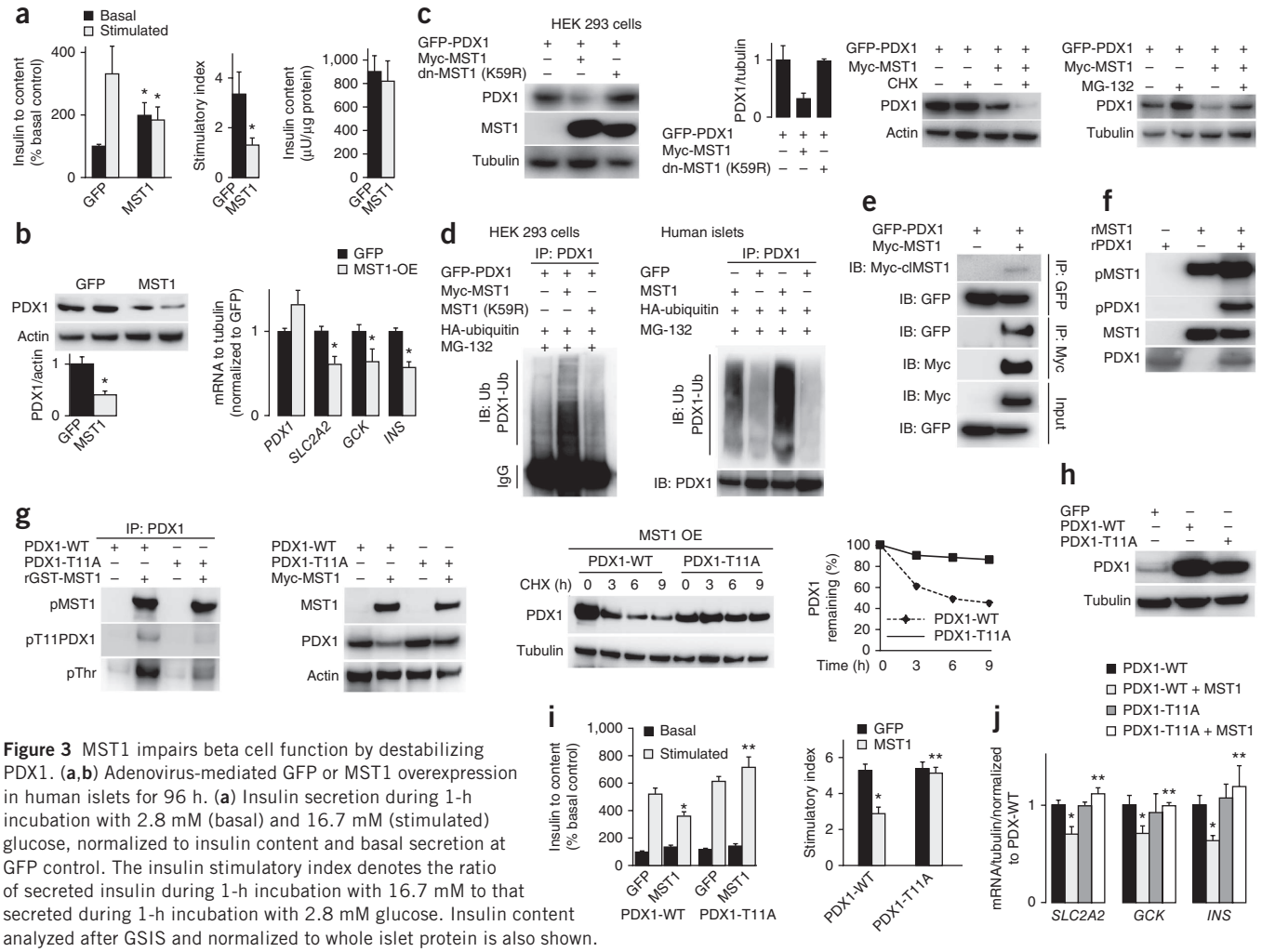

Figure 3 MST1 impairs beta cell function by destabilizing PDX1. (**a**,**b**) Adenovirus-mediated GFP or MST1 overexpression in human islets for 96 h. (**a**) Insulin secretion during 1-h incubation with 2.8 mM (basal) and 16.7 mM (stimulated) glucose, normalized to insulin content and basal secretion at GFP control. The insulin stimulatory index denotes the ratio of secreted insulin during 1-h incubation with 16.7 mM to that secreted during 1-h incubation with 2.8 mM glucose. Insulin content analyzed after GSIS and normalized to whole islet protein is also shown. (**b**) Left, western blot and densitometry analysis of PDX1. Right, RT-PCR analysis of PDX1 target genes *SLC2A2, GCK* and *INS*. (**c**) Western blot and densitometry analysis of PDX1 and MST1 from HEK 293 cells transfected with plasmids encoding Myc-MST1 and GFP-PDX1 with kinase-dead MST1 (dn-MST1, K59R) cotransfected with GFP-PDX1 (left) and western blot of PDX-1 from HEK 293 cells treated with CHX for 8 h at 48 h after transfection, (middle) or treated with the proteasome inhibitor MG-132 for 6 h at 36 h after transfection (right). (**d**) Immunoblotting with ubiquitin-specific antibody after immunoprecipitation with an anti-PDX1 antibody of HEK 293 cells transfected with GFP-PDX1 and hemagglutinin (HA)-ubiquitin (Ub), alone or together with Myc-MST1 or MST1-K59R expression plasmids for 48 h (left) and human islets transfected with HA-ubiquitin and infected with Ad-GFP or Ad-MST1 for 48 h (right; 2 different donors). MG-132 was added during the last 6 h of the experiment. (**e**) Western blot analysis for Myc and GFP with precipitates and input fraction after reciprocal co-immunoprecipitations (using anti-GFP and anti-Myc antibodies) from HEK 293 cells transfected with GFP-PDX1 alone or together with Myc-MST1 for 48 h. (**f**) Western blot of pThr (pan–phosphorylated threonine), MST1 and PDX1 from *in vitro* kinase assay performed with recombinant MST1 (rMST1) and recombinant PDX1 (rPDX1) proteins. (**g**) Left, western blot of pPDX1 (pT11PDX1) and pThr (after immunoprecipitation with anti-PDX1) from HEK 293 cells transfected with PDX1-WT or PDX1-T11A expression plasmids and subjected to an *in vitro* kinase assay using recombinant MST1. Middle, western blot of MST1 and PDX1 from HEK 293 cells transfected with PDX1-WT or PDX1-T11A expression plasmids alone or together with MST1 expression plasmids for 48 h. Right, western blot of PDX1 and densitometry analysis of bands for PDX1-WT or PDX1-T11A cotransfected with MST1 in HEK 293 cells for 36 h and treated with CHX. (**h**) Western blot of PDX1 from human islets transfected with GFP, PDX1-WT or PDX1-T11A expression plasmids. (**i**) Insulin secretion during 1-h incubation with 2.8 mM (basal) and 16.7 mM (stimulated) glucose, normalized to insulin content and basal secretion at control and insulin stimulatory index, which denotes the ratio of secreted insulin during 1-h incubation with 16.7 mM to that secreted at 2.8 mM glucose. (**j**) PDX1 target genes in human islets analyzed by RT-PCR and levels normalized to tubulin and shown as change from PDX1-WT transfected islets from human islets infected with Ad-GFP or Ad-MST1 for 72 h. All western blots show representative results from at least 3 independent experiments from 3 different donors (human islets). Tubulin or actin was used as loading control. RT-PCR (**b**,**j**) and GSIS (**a**,**i**) show pooled results from 3 independent experiments from 3 different donors. Data are expressed as means ± s.e.m. $^{*}P < 0.05$ MST overexpression compared to control, $^{**}P < 0.05$ PDX1-T11A + MST1 compared to PDX1-WT + MST1.

MST1 overexpression had no effect on insulin content (**Fig. 3a** and **Supplementary Fig. 4a**), and thus insulin secretion was normalized on insulin content.

To clarify the mechanism by which MST1 regulates PDX1, we examined the effects of ectopic expression of MST1 and PDX1 in human embryonic kidney (HEK) 293 cells. We found lower PDX1 levels in cells co-overexpressing WT MST1, whereas the kinase-dead MST1-K59R had no effect (**Fig. 3c**). Thus, kinase activity is required for MST1-induced PDX1 degradation. Overexpression of *MST1* also attenuated the transcriptional activity of PDX1 on the rat insulin promoter (RIP), as shown by luciferase assays in PDX1-overexpressing HEK 293 and INS-1E cells (**Supplementary Fig. 4d**).

To discriminate between a transcriptional or translational and a post-translational effect of MST1 on PDX1, we followed the stability of overexpressed PDX1 upon treatment with cycloheximide (CHX), an inhibitor of protein translation. Upon CHX exposure, PDX1 protein levels rapidly decreased when coexpressed with MST1 (**Fig. 3c**), which suggests that MST1 reduced PDX1 protein stability. Consistent with these observations, MST1 overexpression also decreased protein stability of endogenous PDX1 in human islets (**Supplementary Fig. 4e**). In contrast, treatment of PDX1-overexpressing HEK 293 cells with the proteasome inhibitor MG-132 reduced the disappearance of PDX1 (**Fig. 3c**), indicating that MST1 induced activation of the ubiquitin proteasome pathway. Proteasomal degradation of PDX1 has been described before and leads to impaired beta cell function and survival[36].

We next performed *in vivo* ubiquitination assays to determine whether MST1 induces PDX1 ubiquitination. PDX1 cotransfected with MST1, but not with MST1-K59R, was heavily ubiquitinated in HEK 293 cells. We confirmed this in human islets by showing that MST1 overexpression strongly promoted endogenous PDX1 ubiquitination (**Fig. 3d**). Subsequently, we verified a direct interaction between PDX1 and MST1 proteins. Reciprocal co-immunoprecipitations showed the interaction between MST1 and PDX1 in HEK 293 cells cotransfected with GFP-tagged PDX1 and Myc-tagged MST1 (**Fig. 3e**).

We next examined whether a prodiabetic milieu regulates the association between MST1 and PDX1. Notably, both cytokine toxicity and glucotoxicity augment the interaction between MST1 and PDX1 in INS-1E cells (**Supplementary Fig. 4e**). As we observed that PDX1 ubiquitination and degradation required MST1 kinase activity, we tested whether MST1 directly phosphorylates PDX1. *In vitro* kinase assays showed that MST1 efficiently phosphorylated PDX1; these included autoradiography using radiolabeled ^{32}P (**Supplementary Fig. 4f**), as well as nonradioactive kinase assays and western blotting using an antibody specific to pan–phosphorylated threonine (**Fig. 3f**). We confirmed the *in vitro* kinase assays in HEK 293 cells; coexpression of MST1 and PDX1 led to PDX1 phosphorylation (**Supplementary Fig. 4f**). Together, these results establish PDX1 as a substrate for MST1.

We determined the potential MST1-targeted phosphorylation sites on PDX1 theoretically with the NetPhos 2.0 program[37]. This identified six candidate sites within the PDX1 sequence; T11, T126, T152, T155, T214 and T231 (based on the probability that a phosphosite is a substrate of MST1, given as relative score) (**Supplementary Fig. 4g**). These six sites were individually mutated to alanine to generate phosphodeficient constructs as described previously[38]. We subcloned them into pGEX bacterial expression vectors. PDX1-GST fusion proteins with the six different PDX1 mutations were purified from bacteria and used as substrates for MST1 in the kinase assay. With the exception of PDX1-T11A, WT recombinant PDX1 and the other mutants proteins were efficiently phosphorylated at threonine (**Supplementary Fig. 4h**). To confirm this, we transfected all PDX1 mutant plasmids into HEK 293 cells, immunoprecipitated them with a PDX1-specific antibody and incubated them with recombinant MST1 in a kinase assay. MST1 highly phosphorylated PDX1-WT and other mutant proteins, but phosphorylation in the PDX1-T11A mutant was markedly lower (data not shown), indicating that T11 is the major site of phosphorylation by MST1.

In order to confirm T11 as the specific phosphorylation site, we used a phosphospecific antibody against the T11 phosphorylation site in PDX1, which recognized T11 phosphorylation after co-incubation of recombinant PDX1-GST fusion protein with recombinant GST-MST1 (**Supplementary Fig. 4h**). Consistent with this, co-incubation of immunoprecipitated PDX1-WT or PDX1-T11A with recombinant MST1 resulted in robust MST1-induced PDX1-WT phosphorylation at the T11 site (shown by antibody to pT11) and in overall threonine phosphorylation (shown by antibody to pan–phosphorylated threonine); PDX1-T11 phosphorylation was markedly reduced in the PDX1-T11A mutant protein (**Fig. 3g**). We further corroborated this by an *in vivo* kinase assay (**Supplementary Fig. 4h**). Alignment of the amino acid sequences of PDX1 from different species revealed that the T11 site is highly conserved among those species (**Supplementary Fig. 4i**).

If T11 is the specific MST1-induced phosphorylation site of PDX1 and is responsible for beta cell dysfunction, one would expect that mutated PDX1-T11A would reverse beta cell dysfunction. MST1 induced a rapid degradation of exogenous WT PDX1 in the presence of CHX that did not occur in PDX1-T11A mutant–transfected cells (**Fig. 3g**). Furthermore, the half-life of the PDX1-T11A mutant was similar to that of PDX1-WT in the absence of MST1 (data not shown). Consistent with these data, there was less PDX1 ubiquitination in the PDX1-T11A–transfected cells than in those transfected with PDX1-WT (**Supplementary Fig. 4j**).

Because T11 is located within the transactivational domain of PDX1 and to evaluate the functional significance of the T11-dependent ubiquitination and degradation, we assessed transcriptional activity of PDX1. Reduction of PDX1 transcriptional activity occurred only in PDX1-WT– but not in PDX1-T11A–transfected cells (**Supplementary Fig. 4j**). As the T11A mutation of PDX1 prolongs PDX1 stability in the presence of MST1, we asked whether PDX1 stability is directly linked to improved beta cell function. PDX1-T11A mutant overexpression (**Fig. 3h**) normalized MST1-induced impairment in GSIS in human islets (**Fig. 3i**) and INS-1E cells (**Supplementary Fig. 4j**) and restored MST1-induced downregulation of PDX1 target genes (**Fig. 3j** and **Supplementary Fig. 4j**). These findings indicate that MST1-induced PDX1 phosphorylation at T11 leads directly to PDX1 destabilization and impaired beta cell function and suggest that PDX1 is a crucial target of MST1 in the regulation of beta cell function.

MST1 deficiency improves beta cell survival and function

Further analyses aimed to prove whether MST1 not only mediated beta cell death and impaired function *in vitro* but also, when downregulated, allowed for rescue from beta cell failure (**Fig. 4** and **Supplementary Fig. 5**). First, about 80% depletion of MST1 in human islets, achieved with siRNA, protected from cytokine and hydrogen peroxide toxicity as well as glucolipotoxicity; beta cell apoptosis was also inhibited (**Fig. 4a**,**b** and **Supplementary Fig. 5a**). Silencing of *MST1* also significantly reduced BIM upregulation induced by diabetogenic conditions in human islets (**Fig. 4b**,**c** and **Supplementary Fig. 5a**).

Second, beta cell function was greatly improved by *MST1* gene silencing under diabetogenic conditions (**Fig. 4d** and **Supplementary Fig. 5**). Notably, IL/IF- and high glucose + palmitate (HG/Pal)-induced cleavage of caspase-3 and caspase-9 and phosphorylation of H2B was lower in MST1-depleted human islets than in control islets (**Fig. 4b**). *Mst1*$^{-/-}$ islets were largely resistant to IL/IF- and HG/Pal-mediated apoptosis, as determined by TUNEL staining (**Fig. 4e**). In addition to the protective effect of *Mst1* knockout on beta cell survival, *Mst1*$^{-/-}$ islets also showed improved GSIS after long-term culture with IL/IF and HG/Pal (**Fig. 4f** and **Supplementary Fig. 5**). To further support the role of MST1 as a main mediator of apoptosis in beta cells, we generated INS-1E cells stably transfected with vectors carrying *Mst1*-targeting shRNA (sh*Mst1*) or scrambled control shRNA (shScr) and found that Mst1 expression in cells stably expressing sh*Mst1* was about 70% lower than that in cells

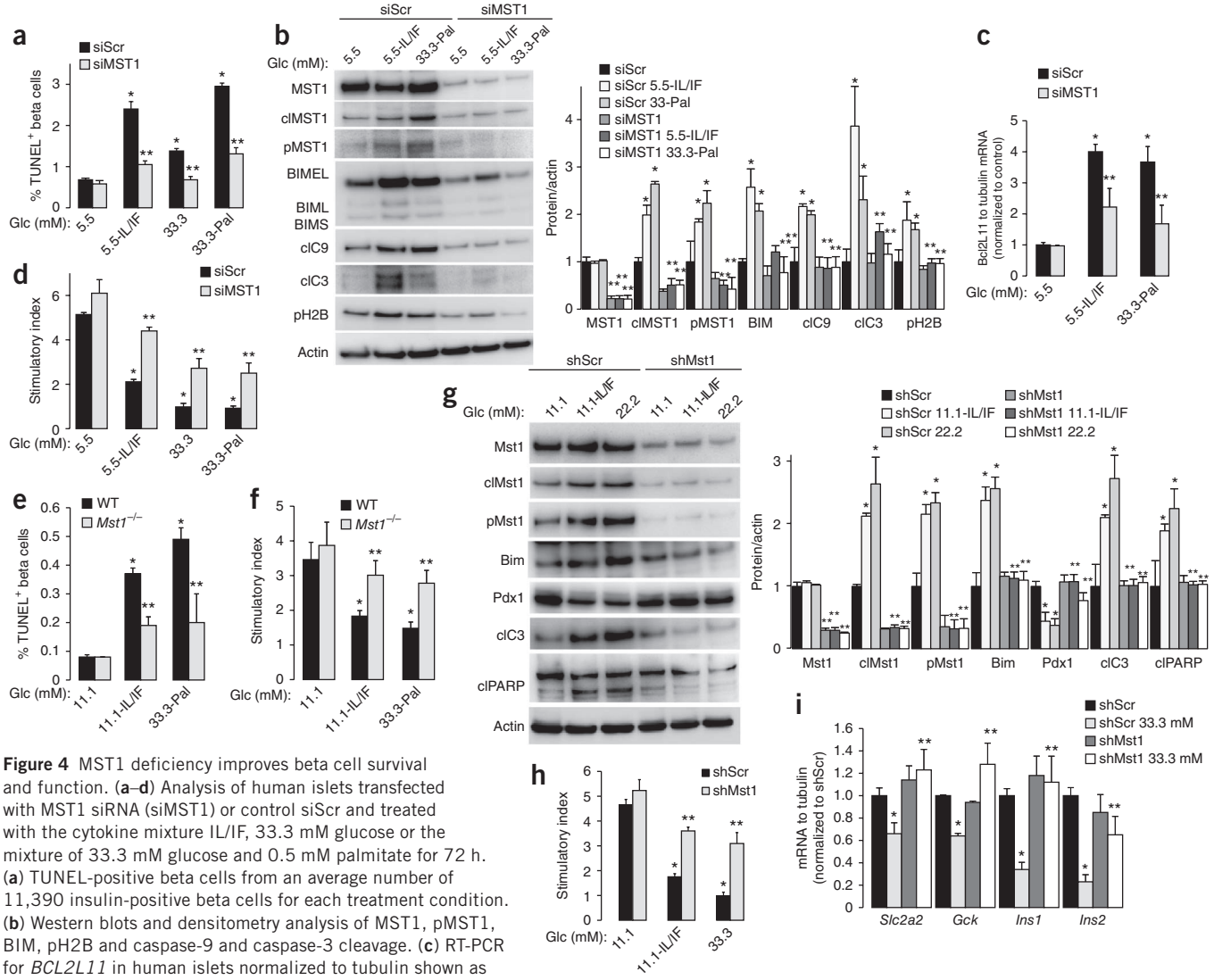

Figure 4 MST1 deficiency improves beta cell survival and function. (**a**–**d**) Analysis of human islets transfected with MST1 siRNA (siMST1) or control siScr and treated with the cytokine mixture IL/IF, 33.3 mM glucose or the mixture of 33.3 mM glucose and 0.5 mM palmitate for 72 h. (**a**) TUNEL-positive beta cells from an average number of 11,390 insulin-positive beta cells for each treatment condition. (**b**) Western blots and densitometry analysis of MST1, pMST1, BIM, pH2B and caspase-9 and caspase-3 cleavage. (**c**) RT-PCR for *BCL2L11* in human islets normalized to tubulin shown as change from siScr control transfected islets. (**d**) Insulin stimulatory index denotes the ratio of secreted insulin during 1-h incubation with 16.7 mM to that secreted during 1-h incubation with 2.8 mM glucose (after the indicated treatments). (**e**) Analysis of TUNEL-positive beta cells from an average number of 24,180 insulin-positive beta cells counted for each treatment condition. (**f**) Insulin stimulatory index denotes the ratio of secreted insulin during 1-h incubation with 16.7 mM to that secreted during 1-h incubation with 2.8 mM glucose from isolated islets from *Mst1*$^{-/-}$ mice and their WT littermates after exposure to the cytokine mixture IL/IF or the mixture of 33.3 mM glucose and 0.5 mM palmitate for 72 h. (**g**–**i**) Western blots and densitometry analysis of Mst1, cIMst1, pMST1, Bim, Pdx1, caspase-3 and PARP cleavage (**g**), insulin stimulatory index (**h**) and RT-PCR analysis of PDX1 target genes *Slc2a2, Gck, Ins1* and *Ins2* normalized to tubulin and shown as change from shScr (**i**) in stable INS-1E clones generated by transfection of vectors for shMst1 and shScr control and treated with the cytokine mixture IL/IF or with 22.2 or 33.3 mM glucose for 72 h. Representative results from 3 independent experiments from 3 different donors (human islets) (**b**,**g**). Actin was used as loading control. TUNEL data (**a**,**e**), GSIS (**d**,**f**,**h**) or RT-PCR (**c**,**i**) show pooled results from 3 independent experiments from 3 different donors (human islets). Data are expressed as means ± s.e.m. $*P < 0.05$ compared to siScr (**a**–**d**), WT (**e**,**f**) or shScr untreated controls (**g**,**h**,**i**); $**P < 0.05$ compared to siScr (**a**–**d**), WT (**e**,**f**) or shScr (**g**–**i**) at the same treatment conditions.

expressing shScr (**Fig. 4g**). We treated INS-1E clones with IL/IF and HG for 72 h. Bim induction, caspase-3 and PARP cleavage in Mst1-depleted cells were significantly lower than that in control cells (**Fig. 4g**). Additionally, *Mst1* silencing also abrogated caspase-3 and PARP cleavage induced by palmitate (**Supplementary Fig. 5b**) and hydrogen peroxide (**Supplementary Fig. 5c**). Cytochrome *c* release was markedly reduced in Mst1-depleted beta cells under diabetogenic conditions (**Supplementary Fig. 5d**,**e**). A second shRNA clone targeting the *Mst1* gene with comparable gene silencing efficiency confirmed the antiapoptotic effect of *Mst1* silencing in INS-1E cells; Mst1 depletion markedly suppressed IL/IF- and HG-induced Bim upregulation and cleavage of caspase-3 and PARP (**Supplementary Fig. 5f**). Confirmation the results of the sh*Mst1* approach, inhibition of endogenous Mst1 activity by overexpression of Mst1-K59R completely inhibited glucose-induced caspase-3 and PARP cleavage in beta cells (**Supplementary Fig. 5g**).

Mst1 deficiency significantly attenuated Pdx1 depletion caused by cytokine or high glucose treatment (**Fig. 4g** and **Supplementary Fig. 5f**), implying that MST1 is indispensable for the reduction in amount of PDX1 induced by a diabetic milieu. Our next objective was to determine whether knockdown of Mst1 expression leads to improvement of GSIS and restoration of Pdx1 target genes in INS-1E cells under diabetogenic conditions. GSIS was significantly improved in Mst1-depleted beta cells (**Fig. 4h** and **Supplementary Fig. 5j**),

whereas levels of Pdx1 target genes, for example, *Slc2a2*, *Gck*, *Ins1* and *Ins2*, were restored in Mst1-depleted INS-1E cells (**Fig. 4i**). These data prove MST1 as determinant for beta cell apoptosis and defective insulin secretion under a diabetic milieu in beta cells *in vitro*.

Mst1 deletion protects from streptozotocin-induced diabetes

As MST1 depletion protected from beta cell apoptosis and restored beta cell function *in vitro*, we hypothesized that Mst1 deficiency may protect against diabetes *in vivo* by promoting beta cell survival and preserving beta cell mass. To test this hypothesis, we used $Mst1^{-/-}$ mice. Neither body weight nor food intake differed between $Mst1^{-/-}$ mice and their WT ($Mst1^{+/+}$) littermates (data not shown). Also, glucose tolerance, insulin tolerance and glucose-induced insulin response did not differ between WT and $Mst1^{-/-}$ mice at 2 months of age (**Supplementary Fig. 6a**). However, intraperitoneal (i.p.) glucose tolerance tests (GTTs) and i.p. insulin tolerance tests (ITTs) revealed slight improvement in $Mst1^{-/-}$ mice at 6 months of age at 60 min after glucose or insulin injection (**Supplementary Fig. 6b**).

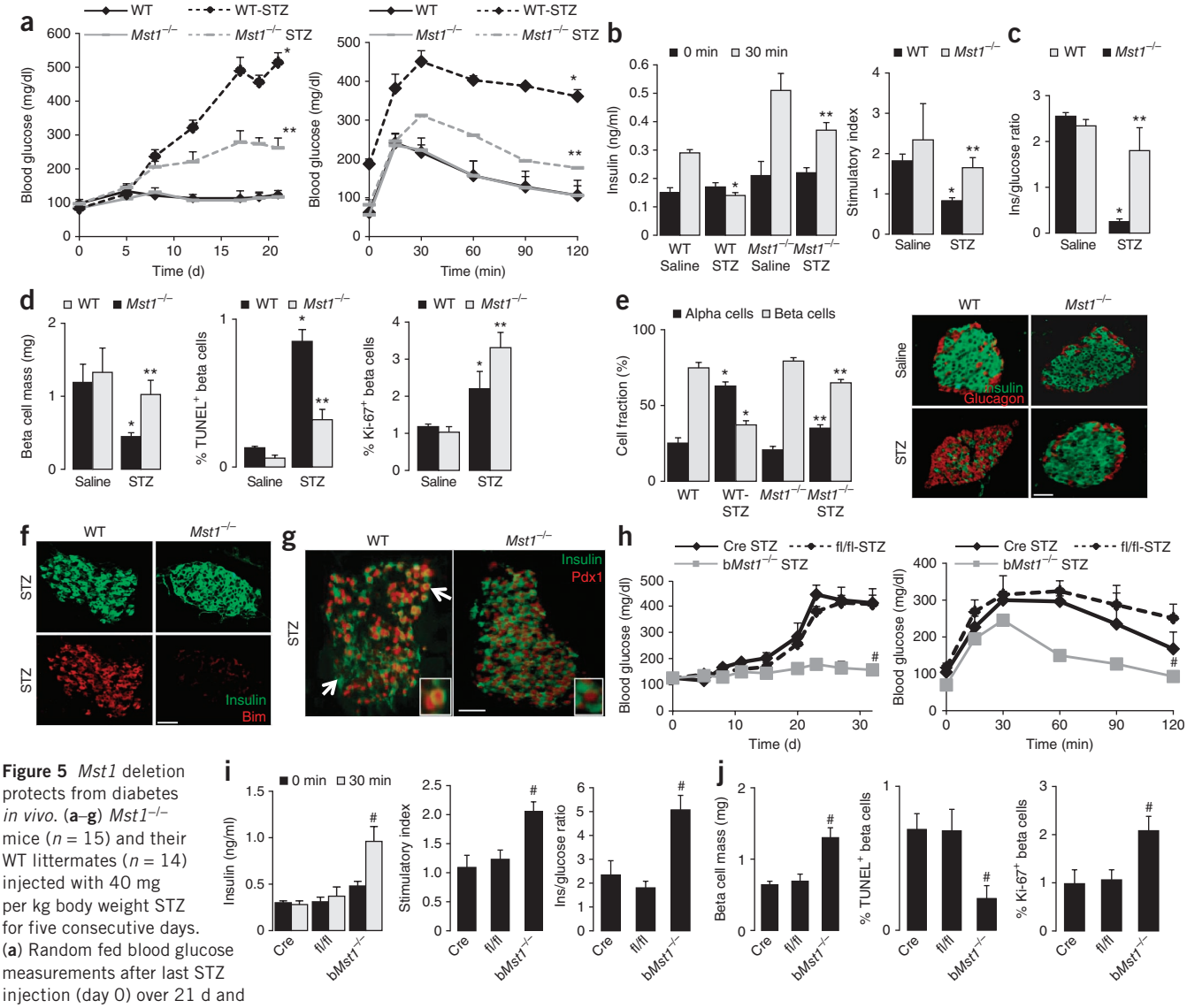

Figure 5 *Mst1* deletion protects from diabetes *in vivo*. (**a**–**g**) $Mst1^{-/-}$ mice ($n = 15$) and their WT littermates ($n = 14$) injected with 40 mg per kg body weight STZ for five consecutive days. (**a**) Random fed blood glucose measurements after last STZ injection (day 0) over 21 d and i.p. GTT (ipGTT) performed at day 17. (**b**) Insulin secretion during an i.p. GTT measured before (0 min) and 30 min after glucose injection (left) expressed as ratio of secreted insulin at 30 min to that secreted at 0 min (stimulatory index, right). (**c**) Ratio of secreted insulin and glucose calculated at fed state. (**d**) Beta cell mass and quantitative analyses from triple stainings for TUNEL or Ki-67, insulin and DAPI expressed as percentage of TUNEL- or Ki-67–positive beta cells ± s.e.m. from a mean scored number of 23,121 beta cells for each treatment condition. (**e**) Percentage of alpha cells (stained in red) and beta cells (stained in green) of the whole pancreatic sections from 10 sections spanning the width of the pancreas. Scale bar, 100 µm. (**f**,**g**) Representative double staining for Bim (red, **f**) or Pdx1 (red, **g**) and insulin (green) from MLD-STZ–treated $Mst1^{-/-}$ mice and controls killed at day 22. White arrows indicate areas of cytosolic Pdx1 localization and its total absence in WT-STZ–treated mice. Scale bars, 100 µm. (**h**–**j**) b$Mst1^{-/-}$ mice with specific deletion in the beta cells using the Cre-*loxP* system ($n = 5$) and RIP-Cre ($n = 3$) and $Mst1^{fl/fl}$ controls ($n = 3$) injected with 40 mg per kg body weight STZ for five consecutive days. (**h**) Random fed blood glucose measurements after last STZ injection (day 0) over 32 d and i.p. GTT at day 30. (**i**) Insulin secretion during an i.p. GTT measured before (0 min) and 30 min after glucose injection. Data are expressed as ratio of secreted insulin at 30 min to that secreted at 0 min (stimulatory index). The ratio of secreted insulin and glucose calculated at fed state (right). (**j**) Beta cell mass, TUNEL or Ki-67 analysis, expressed as percentage of TUNEL- or Ki-67–positive beta cells from mice at day 32. Data show means ± s.e.m. $^{*}P < 0.05$ MLD-STZ–treated WT mice compared to saline-injected WT mice, $^{**}P < 0.05$ MLD-STZ–treated $MST1^{-/-}$ mice compared to MLD-STZ–treated WT mice. $^{\#}P < 0.05$ MLD-STZ–treated b$Mst^{-/-}$ mice compared to MLD-STZ–treated $Mst1^{fl/fl}$ or RIP-Cre mice.

We induced diabetes by multiple low-dose (MLD) streptozotocin (STZ) injections in *Mst1*$^{-/-}$ mice and WT controls. Whereas MLD-STZ injection induced progressive hyperglycemia and severely impaired glucose tolerance in WT mice, blood glucose levels were significantly reduced and glucose tolerance was highly improved in *Mst1*$^{-/-}$ mice (**Fig. 5a**). The MLD-STZ treatment led to impaired insulin secretion and a decreased insulin-to-glucose ratio in WT mice, which were significantly restored in *Mst1*$^{-/-}$ mice (**Fig. 5b**,**c**). Islet architecture in MLD-STZ–treated WT mice was disrupted and accompanied by less insulin-positive area, a smaller beta cell fraction, lower islet density, smaller islet size and lower beta cell mass compared to that of non–MLD-STZ–treated mice. In contrast, islet architecture of MLD-STZ–treated *Mst1*$^{-/-}$ mice had a close to normal appearance, and beta cell fraction, islet density and beta cell mass were similar to those in non–MLD-STZ–treated mice (**Fig. 5d**,**e** and **Supplementary Fig. 6c**). Islet size also tended to be higher in MLD-STZ–injected *Mst1*$^{-/-}$ mice than in WT mice, although this effect was not statistically significant (**Supplementary Fig. 6c**).

To elucidate how MST1 deletion may affect beta cell mass, we studied beta cell apoptosis and proliferation. TUNEL staining demonstrated that the rate of apoptosis was dramatically higher in MLD-STZ–treated WT mice than in treated *Mst1*$^{-/-}$ mice; the *Mst1* deletion markedly lowered the rate of apoptosis. Beta cell proliferation was higher in MLD-STZ–treated WT mice compared to untreated WT mice, but treated *Mst1*$^{-/-}$ beta cells showed even higher proliferation, indicative of an improved compensatory capacity (**Fig. 5d** and **Supplementary Fig. 6d**,**e**). No difference in the frequency of proliferating beta cells was observed between islets from *Mst1*$^{-/-}$ mice and those from their WT littermates at basal levels. These results suggest that *Mst1* deletion boosts beta cell mass and islet density predominantly as a result of lower rates of beta cell apoptosis and higher beta cell proliferation in response to diabetogenic stimulation.

To further assess the effect of MLD-STZ, we performed immunohistochemical analyses of insulin and glucagon on pancreatic sections. Islet cells from MLD-STZ–treated WT mice were architecturally distorted, containing significantly fewer insulin-positive cells and proportionally more glucagon-positive cells, which resulted in a higher alpha cell–to–beta cell ratio compared to untreated WT mice (**Fig. 5e**). This is consistent with the previously reported alpha cell hyperplasia in diabetes[39,40]. In contrast, the number of glucagon-positive alpha cells in MLD-STZ–injected *Mst1*$^{-/-}$ islets was not higher and confined to the rim of the islets, suggesting that the architecture of MLD-STZ–injected *Mst1*$^{-/-}$ islets was close to normal (**Fig. 5e**). In line with our *in vitro* results in beta cells, where MST1 acts through changes in BIM, expression of the latter was clearly seen in beta cells in diabetic MLD-STZ–treated WT mice, but not in treated *Mst1*$^{-/-}$ mice (**Fig. 5f**).

We next examined Pdx1 as a beta cell–specific MST1 substrate whose expression is regulated by both its abundance and its subcellular localization in diabetic conditions[19]. Whereas MLD-STZ–treated WT mice showed a reduced nuclear localization of Pdx1 in beta cells, Pdx1 expression was normalized and the prominent nuclear localization important for its functionality reestablished in MLD-STZ–treated *Mst1*$^{-/-}$ mice (**Fig. 5g**). The expression of the Pdx1 target Glut2 in beta cells was largely preserved in the MLD-STZ–treated *Mst1*$^{-/-}$ mice, whereas it was barely detectable in the beta cells of MLD-STZ–treated WT mice (**Supplementary Fig. 6f**). These findings suggest that *Mst1* deletion preserves Pdx1 and Glut2 expression in beta cells and thus preserves the function of beta cells in the MLD-STZ model of diabetes.

To directly assess the protective effect of *Mst1* deletion in MLD-STZ–induced beta cell apoptosis, we treated isolated mouse islets and INS-1E cells with STZ *in vitro* and found that STZ strongly induced phosphorylation of Mst1, Bim expression and ultimately apoptosis, and such apoptotic induction by STZ was attenuated by Mst1 depletion (**Supplementary Fig. 6g**,**h**), consistent with the *in vivo* observations in *Mst1*$^{-/-}$ mice.

To exclude a secondary effect of the *Mst1* deletion on beta cells, we generated mice with beta cell–specific knockout of *Mst1* by the Cre-*loxP* system (hereafter referred to as b*Mst1*$^{-/-}$ mice). These mice contained a null mutation for *Mst1* only in beta cells, as confirmed by western blotting of lysates from isolated islets (**Supplementary Fig. 7a**). b*Mst1*$^{-/-}$ mice were viable, fertile and showed no difference in food intake and body weight (data not shown), glucose tolerance or insulin sensitivity compared to *Mst1*$^{fl/fl}$ mice, which do not express Cre (**Supplementary Fig. 7b**,**c**), or *loxP*-negative mice (RIP-Cre mice; data not shown). To assess whether b*Mst1*$^{-/-}$ mice might also be protected against diabetes, we again used the model of MLD-STZ–induced diabetes. After MLD-STZ treatment, blood glucose levels in *Mst1*$^{fl/fl}$ and RIP-Cre control mice increased gradually (**Fig. 5h**). Whereas both control groups became overtly diabetic, reaching blood glucose levels >400 mg/dl, b*Mst1*$^{-/-}$ mice maintained normal blood glucose levels. *Mst1*$^{fl/fl}$ and RIP-Cre control mice exhibited impaired glucose tolerance; this was notably prevented in b*Mst1*$^{-/-}$ mice (**Fig. 5h**). This protection was accompanied by significant restoration of glucose-induced insulin response and insulin-to-glucose ratio (**Fig. 5i**). Beta cell protection was also confirmed by the considerably higher beta cell mass in the MLD-STZ–treated b*Mst1*$^{-/-}$ mice, resulting from enhanced beta cell survival and proliferation (**Fig. 5j**), compared to *Mst1*$^{fl/fl}$ and RIP-Cre control mice. These data indicate that beta cell–specific disruption of *Mst1* prevented progressive hyperglycemia and improved glucose tolerance in MLD-STZ–treated mice as a result of less apoptosis and restoration of beta cell mass, suggesting that beta cell–specific activation of Mst1 is a key event in the progressive loss of beta cells in diabetes.

Mst1 deletion protects from HFD-induced diabetes

We further confirmed the protective effect of *Mst1* deletion against hyperglycemia and development of diabetes in a mouse model of T2D. We fed b*Mst1*$^{-/-}$ mice and RIP-Cre controls a normal diet (ND) or a HFD for 20 weeks. Mice fed a HFD gained more weight than the ND-fed group. Beta cell–specific disruption of *Mst1* had an effect on neither weight gain nor food intake in both groups (**Supplementary Fig. 7d**,**e**). HFD feeding increased fed and fasted glucose levels (**Fig. 6a**,**b**) and impaired glucose tolerance (**Fig. 6b**) in the HFD-treated RIP-Cre control mice compared to ND-fed mice, whereas HFD-treated b*Mst1*$^{-/-}$ mice showed significantly lower fed and fasted glucose levels as well as improved glucose tolerance (**Fig. 6a**,**b**).

In RIP-Cre mice on a HFD, insulin secretion during i.p. glucose challenge was markedly attenuated compared with that of the ND-fed group. In contrast, HFD-induced impairment in GSIS was dramatically reversed in mice with beta cell–specific deletion of *Mst1* (**Fig. 6c**). For assessing beta cell glucose responsiveness, we isolated islets from all ND- and HFD-fed groups. Whereas GSIS was severely impaired in islets isolated from HFD-treated RIP-Cre mice compared with ND-treated RIP-Cre mice, islets from b*Mst1*$^{-/-}$ mice remained fully responsive to glucose with improved insulin secretion under the HFD (**Fig. 6d**). Consistent with the improved metabolic phenotype of b*Mst1*$^{-/-}$ mice on HFD, b*Mst1*$^{-/-}$ mice had a higher compensatory beta cell mass relative to WT HFD control mice (**Fig. 6e**). The combination of lower rate of beta cell apoptosis and elevated beta cell proliferation (**Fig. 6e**) in b*Mst1*$^{-/-}$ mice on the HFD, which accounts

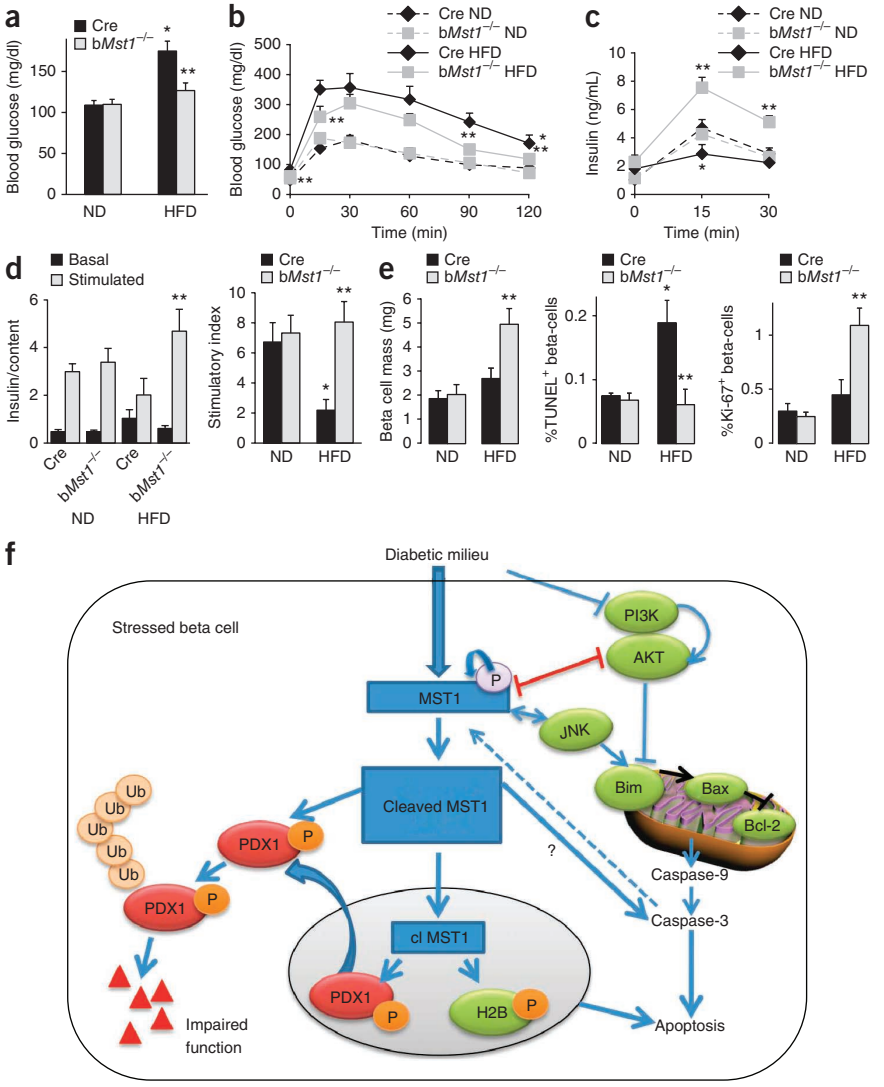

Figure 6 Beta cell–specific disruption of *Mst1* prevents hyperglycemia and HFD-induced diabetes progression. (**a**–**e**) b*Mst1*$^{-/-}$ mice (n = 12) and Cre control mice (n = 12) fed a ND or a HFD diet for 20 weeks. (**a**–**c**) Random fed blood glucose measurements (**a**), i.p. GTT (**b**) and insulin secretion (**c**) during an i.p. GTT measured before (0 min) and 15 and 30 min after glucose injection. (**d**) Insulin secretion during 1-h incubation with 2.8 mM (basal) and 16.7 mM (stimulated) glucose normalized to insulin content from isolated islets from all 4 treatment groups at week 21, cultured overnight and subjected to an *in vitro* GSIS assay. The insulin stimulatory index denotes the ratio of secreted insulin during 1-h incubation with 16.7 mM to secreted insulin at 2.8 mM glucose. (**e**) Beta cell mass, TUNEL and Ki-67 analysis expressed as percentage of TUNEL- or Ki-67–positive beta cells ± s.e.m. from a mean number of 28,521 scored beta cells for each treatment condition. *P < 0.05 HFD-fed Cre mice (Cre HFD) compared to ND-fed Cre mice (Cre ND). **P < 0.05 HFD-fed b*Mst1*$^{-/-}$ mice (b*Mst1*$^{-/-}$ HFD) compared to HFD-fed Cre mice (Cre HFD). (**f**) Our view on how diabetic stimuli lead to activation of MST1. Active MST1 triggers cytochrome *c* release and mitochondrial-dependent apoptosis by modulating Bim/Bax/Bcl-2/Bcl-xL through JNK-AKT signaling. Active caspase-9 then triggers cleavage of caspase-3, which triggers the caspase-3–dependent cleavage of MST1 to its constitutively active fragment, which leads to further MST1 activation and processing of caspase-3 by a positive feedback mechanism, and acceleration of beta cell death occurs. Cleaved MST1 translocates to the nucleus and directly phosphorylates PDX1 (we do not exclude the possibility that MST1 targets PDX1 also in cytoplasm) and histone H2B. PDX1 then shuttles to cytosol, where it undergoes ubiquitination and subsequent degradation by proteasome machinery, and beta cell function is impaired. Histone H2B phosphorylation by MST1 also induces chromatin condensation, one of the characteristic features of apoptosis.

for the higher beta cell mass in b*MST1*$^{-/-}$ mice under the HFD, correlates with the improved glucose tolerance and insulin secretion. This is also supported by results from an i.p. ITT: glucose levels were normalized to the basal levels before insulin injection, and b*Mst1*$^{-/-}$ mice and RIP-Cre control mice on HFD showed a similar impairment in insulin sensitivity (**Supplementary Fig. 7f**,**g**).

To test whether knockdown of MST1 expression could directly rescue beta cells, we transfected islets isolated from 10-week-old obese *db/db* mice and their heterozygous littermates with scrambled control siRNA or *Mst1* siRNA. Whereas Scr siRNA–treated isolated islets from *db/db* mice showed low Pdx1 expression and high caspase-3 cleavage and Bim expression, *Mst1* silencing restored Pdx1, inhibited Bim upregulation and dramatically reduced caspase-3 cleavage (**Supplementary Fig. 8**).

DISCUSSION

Our work shows that MST1 acts as an essential apoptotic molecule in the presence of diabetic stimuli and is a common component in the diverse signaling pathways leading to impaired beta cell survival in diabetes. We identified PDX1 as a beta cell–specific substrate for MST1. PDX1 ubiquitination and subsequent degradation, resulting from inhibitory T11 phosphorylation, is crucial for beta cell dysfunction after MST1 hyperactivation in diabetes (**Fig. 6f**). Deletion of *Mst1* preserves beta cell function and survival providing protection from diabetic insults.

MST1 has a central role in the initiation of cell death[9,41–44]. In line with our data, *Mst1* ablation *in vivo* resulted in resistance to apoptosis induced by tumor necrosis factor-α[45], Fas ligand[46] or IFN-γ[47]. Notably, suppression of endogenous Mst1 by cardiac-specific overexpression of the dominant-negative form of MST1 prevented cardiomyocyte death induced by ischemia-reperfusion[48], which supports the pathophysiological significance of MST1. The diversity of diabetic stimuli by which MST1 is activated in beta cells suggests that this enzyme may be a common component in the many signaling pathways leading to beta cell apoptosis. Although the endogenous molecules that trigger MST1 activation remain unknown, we show that MST1 is highly active in a diabetic environment and induces the mitochondrial-dependent apoptosis pathway in beta cells through targeting BIM, which leads to alterations in BCL-2/BAX or BCL-xL/BAX ratios, cytochrome *c* release, subsequent caspase-9 and caspase-3 cleavage and cell death.

The PI3K-AKT pathway has a critical role in the regulation of beta cell survival. AKT-mediated phosphorylation of multiple substrates positively regulates insulin transcription, insulin secretion and beta cell growth and survival[21,22,49]. Recent studies suggest potential crosstalk between MST1 and AKT[23,24]. MST1 activity is negatively regulated by AKT-mediated phosphorylation at its T120 and T387 residues, which results in inhibition of its cleavage, autophosphorylation, kinase activity and nuclear translocation[23]. On the other hand, MST1 and its cleaved form interact with AKT1 and act as direct AKT1 inhibitors[24]. Our data demonstrate that activation of the PI3K-AKT pathway in beta cells abrogates glucose- and cytokine-induced MST1 activation and beta cell apoptosis, whereas suppression of PI3K-AKT signaling induces MST1 activity and beta cell apoptosis. AKT and MST1 are components of two parallel stress-triggered signaling pathways that functionally antagonize each other. Activated AKT itself downregulates MST1 function in beta cells, indicating the existence of a potential bidirectional crosstalk between these two pathways. Here, we show that MST1 and AKT negatively regulate each other and constitute a stress-sensitive survival pathway. Under acute stress conditions, AKT promoted cell survival by inhibiting MST1, but prolonged stress decreased AKT activity, which allowed for proapoptotic MST1 signaling.

MST1 may affect signal pathways of diabetic stimuli through modulation of transcription factors and gene expression profiles that initiate the process of beta cell failure. In this study, we show that MST1 can physically interact with and phosphorylate PDX1. Targeted disruption of PDX1 in beta cells leads to diabetes, and reducing its expression affects insulin expression and secretion[50]. We have identified the T11 residue of PDX1 as the phosphorylation site used by MST1. Such a kinase-dependent function would be consistent with the comparably low level of PDX1 and high levels of active MST1 in stressed beta cells and pancreases of diabetic mice in our study. PDX1 is restored by deletion of *Mst1* under diabetic conditions. T11 is found in the highly conserved region of PDX1 at the transcription activation domain. T11 phosphorylation of PDX1 by MST1 marks PDX1 for degradation by the proteasome machinery, which would prohibit it from functioning as a transcription factor in the nucleus. In that regard, overexpression of MST1 caused reduction of PDX1 target gene expression and impairment of beta cell function, as assessed by GSIS, whereas mutation of the T11 site allowed PDX1 to be more stabilized and resistant to MST1-induced degradation, restoring PDX1-induced gene expression and improvement of beta cell function. The same site (T11) was previously shown to be targeted by DNA-dependent protein kinase. Consistent with our data, phosphorylation of PDX1 by this kinase results in enhanced PDX1 protein degradation[51]. PDX1 is degraded by the ubiquitin-proteasome pathway; PDX1 C terminal–inhibiting factor-1 (PCIF1) targets PDX1 for ubiquitination and proteasomal degradation by the E3 ubiquitin ligase cullin 3. Ubiquitination of PDX1 regulates its activity, as Pcif1 deficiency normalizes Pdx1 protein levels and improves glucose homeostasis and beta cell function in *Pdx1*$^{+/-}$ mice[36]. Notably, accumulation of polyubiquinated proteins was higher in beta cells of individuals with T2D than in nondiabetic controls[52], highlighting that higher expression of polyubiquinated proteins may contribute to beta cell dysfunction under diabetic conditions.

In mammals, the absolute number of beta cells reflects a dynamic balance between beta cell growth and death. An inadequate expansion of beta cell mass to compensate for the increased insulin demand, followed by the eventual loss of beta cells due to apoptosis, is a hallmark of diabetes[4,53]. This is most apparent in T1D when ongoing autoimmunity causes destruction and consequent loss of beta cells. Through deletion of the MST1-mediated death signal, we have uncovered a deleterious action of MST1 that induces apoptosis in response to diabetic injuries in the immune-mediated beta cell destruction in the MLD-STZ model, a model of beta cell demise that occurs in the absence of insulin resistance. *Mst1* deletion not only prevents MLD-STZ–induced beta cell death but also improves the capacity of beta cells to produce insulin. *Mst1* deletion preserves beta cell mass, improves beta cell function and prevents islet deterioration, as shown by the maintenance of the islet structure, density, size and mass. The observed ability to preserve islet appearance is associated with a protective role for Mst1 deficiency in MLD-STZ–induced beta cell death and in enhancing beta cell proliferation.

Preservation of PDX1 is one mechanism involved in the protection of beta cells by MST1 depletion. This conclusion is strongly supported by our *in vitro* and *in vivo* data; Pdx1 target gene expression is normalized and Glut2 localization is preserved in *Mst1*$^{-/-}$ mice. As both Pdx1 and Glut2 are involved in glucose sensing and GSIS, *Mst1*$^{-/-}$ mice show normal blood glucose levels and high circulating insulin concentrations. STZ enters beta cells via Glut2. It is unlikely that the resistance of *Mst1*$^{-/-}$ mice to MLD-STZ–induced beta cell damage is due to changes in membrane Glut2 expression in beta cells because *Mst1* deletion did not reduce membrane expression of Glut2 in beta cells in mice without STZ treatments.

The high rate of apoptosis in the Mst1-deficient thymocytes further illustrates the cell type–specific variation in the outputs of MST1 signaling. Whereas in thymocytes and T cells deletion of *Mst1* increases the apoptosis rate[54–56], possibly through high levels of reactive oxygen species, Mst1-deficient hepatocytes and microglia exhibit a marked resistance to stress-induced apoptosis[46,47]. Thus, the consequences of Mst1 deficiency need to be established in each cell type and tissue. We used a tissue-specific gene-targeting approach in the current study to provide insights into the biological role of Mst1 in beta cells *in vivo*. It is known that activation and migration of both T cells and macrophages play an important part in islet destruction leading to hyperglycemia in the MLD-STZ model[57]. Infiltrating macrophages and T cells are a major source of the proinflammatory cytokines that promote islet destruction. Thus, the depletion of peripheral T cells in *Mst1*$^{-/-}$ mice[54,55] might be a reason for their protection from MLD-STZ–induced hyperglycemia. We cannot exclude such T cell depletion in our model, but if it occurs, it only has a minor role, as beta cell–specific deletion of *Mst1* in mice completely protected them from hyperglycemia and islet destruction. This shows that *Mst1* ablation in beta cells, but not in other tissues, is a major reason for the protection from MLD-STZ–induced diabetes. Notably, beta cell–specific deletion of *Mst1* in this model led to protection against beta cell apoptosis and diabetes, further underlining the critical role of MST1 in beta cell survival.

The detrimental effects of a long-term HFD on beta cell function and insulin sensitivity leading to glucose intolerance and T2D in mice have been clearly established[58]. As expected, long-term HFD feeding was associated with insulin resistance, glucose intolerance, beta cell dysfunction and loss of compensatory beta cell adaptation. As observed in the MLD-STZ model, in the HFD diabetes model, beta cell–specific *Mst1* deletion results in improved glucose tolerance, insulin secretion and beta cell mass as a result of improved beta cell survival and proliferation, whereas insulin sensitivity is not affected. We have not investigated whether Mst1 is also activated in other organs during diabetes progression, but activated Mst1 has been found in the kidneys of hyperglycemic insulin receptor substrate-2 knockout mice[59] and in epididymal fat pads of HFD-treated mice[60].

Our findings raise the possibility that MST1 hyperactivity is associated with beta cell failure and development of diabetes. Current therapies for the treatment of diabetes mellitus are directed toward alleviating the symptoms of the disease, but there is an urgent medical need for therapies that slow or prevent the loss (rapid in T1D, progressive in T2D) of functional pancreatic beta cell mass. In light of the critical role of MST1 in beta cell failure and initiation of pro-diabetic milieu–induced apoptotic signaling, therapeutic strategies designed to inhibit MST1 activity may both protect beta cells against the effects of autoimmune attack in T1D and preserve beta cell mass and function in T2D.

METHODS

Methods and any associated references are available in the online version of the paper.

Note: Any Supplementary Information and Source Data files are available in the online version of the paper.

ACKNOWLEDGMENTS

This work was supported by the JDRF, the German Research Foundation (Emmy Noether Programm MA4172/1-1), the European Research Council, the German Federal Ministry of Science (Diabetes Competence Network), the European Federation for the Study of Diabetes and University of Bremen Research Funds (all to K.M.). We thank J. Bergemann for excellent technical assistance, G. Dharmadhikari and M. Panse for help with the analyses and G. Rutter and D. Schumann for critical discussion. Human islets were provided through the Juvenile Diabetes Research Foundation award 31-2008-413 (European Consortium for Islet Transplantation Islets for Basic Research Program) and by the Integrated Islet Distribution Program. Human pancreatic sections were obtained from the National Disease Research Interchange, which is supported by the US National Institutes of Health. MST1 and dn-MST1 plasmids and adenoviruses were provided by J. Sadoshima and Y. Maejima (Rutgers New Jersey Medical School), PDX1-WT plasmids and pGEX bacterial expression vector by R. Walther (University of Greifswald), INS-1E cells by C. Wollheim (Lund and Geneva Universities), RIP-Cre mice by P. Herrera (University of Geneva) and A. Mansouri (Max Planck Institute for Biophysical Chemistry), mouse pB.RSV.PDX1-GFP plasmid by I. Leibiger (Karolinska University) and rat insulin-2 promoter plasmid by R. Zinkernagel (University of Zurich). Adenovirus carrying eGFP as a control was provided by A.E. Karlsen (Novo Nordisk A/S).

AUTHOR CONTRIBUTIONS

A.A. conceived of the project, designed all and performed most of the experiments, analyzed the data and wrote the paper. F. Paroni provided experimental and technical support and analyzed data. Z.A., S.K., V.K. and T.Y. performed experiments and analyzed data. T.F. provided mutated PDX1 plasmids, W.T. provided *Mst1*$^{-/-}$ and *Mst1*$^{fl/fl}$ mice and J.K.C., F. Pattou and J.O. isolated human islets. K.M. supervised the project and wrote the paper.

COMPETING FINANCIAL INTERESTS

The authors declare no competing financial interests.

1. Kurrer, M.O., Pakala, S.V., Hanson, H.L. & Katz, J.D. Beta cell apoptosis in T cell–mediated autoimmune diabetes. *Proc. Natl. Acad. Sci. USA* **94**, 213–218 (1997).
2. Mathis, D., Vence, L. & Benoist, C. Beta-cell death during progression to diabetes. *Nature* **414**, 792–798 (2001).
3. Butler, A.E. *et al.* Beta-cell deficit and increased beta-cell apoptosis in humans with type 2 diabetes. *Diabetes* **52**, 102–110 (2003).
4. Rhodes, C.J. Type 2 diabetes—a matter of beta-cell life and death? *Science* **307**, 380–384 (2005).
5. Donath, M.Y., Storling, J., Maedler, K. & Mandrup-Poulsen, T. Inflammatory mediators and islet beta-cell failure: a link between type 1 and type 2 diabetes. *J. Mol. Med.* **81**, 455–470 (2003).
6. The Diabetes Control and Complications Trial Research Group. Effect of intensive therapy on residual beta-cell function in patients with type 1 diabetes in the diabetes control and complications trial. A randomized, controlled trial. *Ann. Intern. Med.* **128**, 517–523 (1998).
7. Lenzen, S., Drinkgern, J. & Tiedge, M. Low antioxidant enzyme gene expression in pancreatic islets compared with various other mouse tissues. *Free Radic. Biol. Med.* **20**, 463–466 (1996).
8. Ling, P., Lu, T.J., Yuan, C.J. & Lai, M.D. Biosignaling of mammalian Ste20-related kinases. *Cell. Signal.* **20**, 1237–1247 (2008).
9. Avruch, J. *et al.* Protein kinases of the Hippo pathway: regulation and substrates. *Semin. Cell Dev. Biol.* **23**, 770–784 (2012).
10. Lee, K.K. *et al.* Proteolytic activation of MST/Krs, STE20-related protein kinase, by caspase during apoptosis. *Oncogene* **16**, 3029–3037 (1998).
11. Kakeya, H., Onose, R. & Osada, H. Caspase-mediated activation of a 36-kDa myelin basic protein kinase during anticancer drug-induced apoptosis. *Cancer Res.* **58**, 4888–4894 (1998).
12. Bi, W. *et al.* c-Jun N-terminal kinase enhances MST1-mediated pro-apoptotic signaling through phosphorylation at serine 82. *J. Biol. Chem.* **285**, 6259–6264 (2010).
13. Cheung, W.L. *et al.* Apoptotic phosphorylation of histone H2B is mediated by mammalian sterile twenty kinase. *Cell* **113**, 507–517 (2003).
14. Jonsson, J., Carlsson, L., Edlund, T. & Edlund, H. Insulin-promoter-factor 1 is required for pancreas development in mice. *Nature* **371**, 606–609 (1994).
15. Stoffers, D.A., Zinkin, N.T., Stanojevic, V., Clarke, W.L. & Habener, J.F. Pancreatic agenesis attributable to a single nucleotide deletion in the human *IPF1* gene coding sequence. *Nat. Genet.* **15**, 106–110 (1997).
16. Johnson, J.D. *et al.* Increased islet apoptosis in *Pdx1*$^{+/-}$ mice. *J. Clin. Invest.* **111**, 1147–1160 (2003).
17. Stoffers, D.A., Ferrer, J., Clarke, W.L. & Habener, J.F. Early-onset type-II diabetes mellitus (MODY4) linked to IPF1. *Nat. Genet.* **17**, 138–139 (1997).
18. Brissova, M. *et al.* Reduction in pancreatic transcription factor PDX-1 impairs glucose-stimulated insulin secretion. *J. Biol. Chem.* **277**, 11225–11232 (2002).
19. Ardestani, A. *et al.* Neutralizing interleukin-1β (IL-1β) induces beta cell survival by maintaining PDX1 protein nuclear localization. *J. Biol. Chem.* **286**, 17144–17155 (2011).
20. Lee, K.K., Ohyama, T., Yajima, N., Tsubuki, S. & Yonehara, S. MST, a physiological caspase substrate, highly sensitizes apoptosis both upstream and downstream of caspase activation. *J. Biol. Chem.* **276**, 19276–19285 (2001).
21. Tuttle, R.L. *et al.* Regulation of pancreatic beta-cell growth and survival by the serine/threonine protein kinase Akt1/PKBα. *Nat. Med.* **7**, 1133–1137 (2001).
22. Bernal-Mizrachi, E., Wen, W., Stahlhut, S., Welling, C.M. & Permutt, M.A. Islet beta cell expression of constitutively active Akt1/PKB α induces striking hypertrophy, hyperplasia, and hyperinsulinemia. *J. Clin. Invest.* **108**, 1631–1638 (2001).
23. Yuan, Z. *et al.* Phosphoinositide 3-kinase/Akt inhibits MST1-mediated pro-apoptotic signaling through phosphorylation of threonine 120. *J. Biol. Chem.* **285**, 3815–3824 (2010).
24. Cinar, B. *et al.* The pro-apoptotic kinase Mst1 and its caspase cleavage products are direct inhibitors of Akt1. *EMBO J.* **26**, 4523–4534 (2007).
25. Trümper, K. *et al.* Integrative mitogenic role of protein kinase B/Akt in beta-cells. *Ann. NY Acad. Sci.* **921**, 242–250 (2000).
26. Matallanas, D. *et al.* RASSF1A elicits apoptosis through an MST2 pathway directing proapoptotic transcription by the p73 tumor suppressor protein. *Mol. Cell* **27**, 962–975 (2007).
27. Valis, K. *et al.* Hippo/Mst1 stimulates transcription of the proapoptotic mediator NOXA in a FoxO1-dependent manner. *Cancer Res.* **71**, 946–954 (2011).
28. Grunnet, L.G. *et al.* Proinflammatory cytokines activate the intrinsic apoptotic pathway in beta-cells. *Diabetes* **58**, 1807–1815 (2009).
29. Opferman, J.T. & Korsmeyer, S.J. Apoptosis in the development and maintenance of the immune system. *Nat. Immunol.* **4**, 410–415 (2003).
30. Yamamoto, S. *et al.* Activation of Mst1 causes dilated cardiomyopathy by stimulating apoptosis without compensatory ventricular myocyte hypertrophy. *J. Clin. Invest.* **111**, 1463–1474 (2003).
31. Lei, K. & Davis, R.J. JNK phosphorylation of Bim-related members of the Bcl2 family induces Bax-dependent apoptosis. *Proc. Natl. Acad. Sci. USA* **100**, 2432–2437 (2003).
32. Rahmani, M. *et al.* The BH3-only protein Bim plays a critical role in leukemia cell death triggered by concomitant inhibition of the PI3K/Akt and MEK/ERK1/2 pathways. *Blood* **114**, 4507–4516 (2009).
33. Humphrey, R.K., Yu, S.M., Flores, L.E. & Jhala, U.S. Glucose regulates steady-state levels of PDX1 via the reciprocal actions of GSK3 and AKT kinases. *J. Biol. Chem.* **285**, 3406–3416 (2010).
34. Kawamori, D. *et al.* The forkhead transcription factor Foxo1 bridges the JNK pathway and the transcription factor PDX-1 through its intracellular translocation. *J. Biol. Chem.* **281**, 1091–1098 (2006).
35. McCulloch, L.J. *et al.* GLUT2 (SLC2A2) is not the principal glucose transporter in human pancreatic beta cells: implications for understanding genetic association signals at this locus. *Mol. Genet. Metab.* **104**, 648–653 (2011).
36. Claiborn, K.C. *et al.* Pcif1 modulates Pdx1 protein stability and pancreatic beta cell function and survival in mice. *J. Clin. Invest.* **120**, 3713–3721 (2010).
37. Miller, M.L. *et al.* Linear motif atlas for phosphorylation-dependent signaling. *Sci. Signal.* **1**, ra2 (2008).
38. Frogne, T., Sylvestersen, K.B., Kubicek, S., Nielsen, M.L. & Hecksher-Sorensen, J. Pdx1 is post-translationally modified *in vivo* and serine 61 is the principal site of phosphorylation. *PLoS ONE* **7**, e35233 (2012).
39. Dunning, B.E. & Gerich, J.E. The role of alpha cell dysregulation in fasting and postprandial hyperglycemia in type 2 diabetes and therapeutic implications. *Endocr. Rev.* **28**, 253–283 (2007).

40. Li, Z., Karlsson, F.A. & Sandler, S. Islet loss and alpha cell expansion in type 1 diabetes induced by multiple low-dose streptozotocin administration in mice. *J. Endocrinol.* **165**, 93–99 (2000).
41. Lin, Y., Khokhlatchev, A., Figeys, D. & Avruch, J. Death-associated protein 4 binds MST1 and augments MST1-induced apoptosis. *J. Biol. Chem.* **277**, 47991–48001 (2002).
42. Del Re, D.P. *et al.* Proapoptotic Rassf1A/Mst1 signaling in cardiac fibroblasts is protective against pressure overload in mice. *J. Clin. Invest.* **120**, 3555–3567 (2010).
43. Graves, J.D., Draves, K.E., Gotoh, Y., Krebs, E.G. & Clark, E.A. Both phosphorylation and caspase-mediated cleavage contribute to regulation of the Ste20-like protein kinase Mst1 during CD95/Fas-induced apoptosis. *J. Biol. Chem.* **276**, 14909–14915 (2001).
44. Graves, J.D. *et al.* Caspase-mediated activation and induction of apoptosis by the mammalian Ste20-like kinase Mst1. *EMBO J.* **17**, 2224–2234 (1998).
45. Song, H. *et al.* Mammalian Mst1 and Mst2 kinases play essential roles in organ size control and tumor suppression. *Proc. Natl. Acad. Sci. USA* **107**, 1431–1436 (2010).
46. Zhou, D. *et al.* Mst1 and Mst2 maintain hepatocyte quiescence and suppress hepatocellular carcinoma development through inactivation of the Yap1 oncogene. *Cancer Cell* **16**, 425–438 (2009).
47. Yun, H.J. *et al.* Daxx mediates activation-induced cell death in microglia by triggering MST1 signalling. *EMBO J.* **30**, 2465–2476 (2011).
48. Odashima, M. *et al.* Inhibition of endogenous Mst1 prevents apoptosis and cardiac dysfunction without affecting cardiac hypertrophy after myocardial infarction. *Circ. Res.* **100**, 1344–1352 (2007).
49. Assmann, A., Ueki, K., Winnay, J.N., Kadowaki, T. & Kulkarni, R.N. Glucose effects on beta-cell growth and survival require activation of insulin receptors and insulin receptor substrate 2. *Mol. Cell. Biol.* **29**, 3219–3228 (2009).
50. Ahlgren, U., Jonsson, J., Jonsson, L., Simu, K. & Edlund, H. beta-cell–specific inactivation of the mouse Ipf1/Pdx1 gene results in loss of the beta-cell phenotype and maturity onset diabetes. *Genes Dev.* **12**, 1763–1768 (1998).
51. Lebrun, P., Montminy, M.R. & Van Obberghen, E. Regulation of the pancreatic duodenal homeobox-1 protein by DNA-dependent protein kinase. *J. Biol. Chem.* **280**, 38203–38210 (2005).
52. Costes, S. *et al.* Beta-cell dysfunctional ERAD/ubiquitin/proteasome system in type 2 diabetes mediated by islet amyloid polypeptide-induced UCH-L1 deficiency. *Diabetes* **60**, 227–238 (2011).
53. Butler, P.C., Meier, J.J., Butler, A.E. & Bhushan, A. The replication of beta cells in normal physiology, in disease and for therapy. *Nat. Clin. Pract. Endocrinol. Metab.* **3**, 758–768 (2007).
54. Choi, J. *et al.* Mst1-FoxO signaling protects naive T lymphocytes from cellular oxidative stress in mice. *PLoS ONE* **4**, e8011 (2009).
55. Dong, Y. *et al.* A cell-intrinsic role for Mst1 in regulating thymocyte egress. *J. Immunol.* **183**, 3865–3872 (2009).
56. Ueda, Y. *et al.* Mst1 regulates integrin-dependent thymocyte trafficking and antigen recognition in the thymus. *Nat. Commun.* **3**, 1098 (2012).
57. Soltani, N. *et al.* GABA exerts protective and regenerative effects on islet beta cells and reverses diabetes. *Proc. Natl. Acad. Sci. USA* **108**, 11692–11697 (2011).
58. Sauter, N.S., Schulthess, F.T., Galasso, R., Castellani, L.W. & Maedler, K. The antiinflammatory cytokine interleukin-1 receptor antagonist protects from high-fat diet–induced hyperglycemia. *Endocrinology* **149**, 2208–2218 (2008).
59. Carew, R.M. *et al.* Deletion of Irs2 causes reduced kidney size in mice: role for inhibition of GSK3β? *BMC Dev. Biol.* **10**, 73 (2010).
60. Kawano, Y. *et al.* Loss of Pdk1-Foxo1 signaling in myeloid cells predisposes to adipose tissue inflammation and insulin resistance. *Diabetes* **61**, 1935–1948 (2012).

ONLINE METHODS

Cell culture, treatment and islet isolation. Human islets were isolated from twenty pancreases of healthy organ donors and from five with T2D at the University of Illinois at Chicago or Lille University and cultured on extracellular matrix (ECM)-coated dishes (Novamed, Jerusalem, Israel) as described previously[61]. Informed consent was obtained from all subjects. Islet purity was greater than 95% as judged by dithizone staining (if this degree of purity was not achieved by routine isolation, islets were handpicked). Ethical approval for the use of human islets had been granted by the Ethics Committee of the University of Bremen. Islets from *Mst1*$^{-/-}$ mice and their WT littermates were isolated as described previously[61]. Pancreases were perifused with a Liberase TM (#05401119001, Roche, Mannheim, Germany) solution according to the manufacturer's instructions and digested at 37 °C, followed by washing and handpicking. The clonal rat beta cell line INS-1E was provided by C. Wollheim. Human islets were cultured in complete CMRL-1066 (Invitrogen) medium at 5.5 mM glucose, mouse islets and INS-1E cells were cultured in complete RPMI-1640 medium at 11.1 mM glucose and HEK 293 cells were cultured in DMEM. All media included glutamate, 1% penicillin-streptomycin and 10% FBS (all from PAA). INS-1E medium was supplemented with 10 mM HEPES, 1 mM sodium pyruvate and 50 μM β-mercaptoethanol. Islets and INS-1E cells were exposed to complex diabetogenic conditions: 22.2 or 33.3 mM glucose, 0.5 mM palmitic acid or the mixture of 2 ng/ml recombinant human IL-1β (R&D Systems, Minneapolis, MN) plus 1,000 U/ml recombinant human IFN-γ (PeproTech) for 72 h, 100 μM H_2O_2 for 6 h, 1 mM streptozotocin (STZ) for 8 h or 1 mM thapsigargin for 6 h (all Sigma). In some experiments, cells were additionally cultured with 10–25 μM JNK-selective inhibitor SP600125, 10 μM PI3K-selective inhibitor LY294002, 10 or 20 μM AKT inhibitor V, triciribine, a selective AKT1/2/3 inhibitor, 50 μM pancaspase inhibitor Z-VAD (OMe)-fmk, 100 μM Bax-inhibiting peptide V5 or Bax-inhibiting peptide, negative control, 20 μM InSolution MG-132, proteasome inhibitor (all Calbiochem), 100 nM glucagon like-peptide 1 (GLP1), 100 nM recombinant human insulin and 50 μg/ml cycloheximide (CHX) and 1 μM glibenclamide (all Sigma). Palmitic acid was dissolved as described previously[62].

Mice. For MLD-STZ experiments, 8- to 10-week old *Mst1*$^{-/-}$ mice on a 129/sv genetic background[55] and their *Mst1*$^{+/+}$ WT littermates were i.p. injected with STZ (40 mg per kg body weight; Sigma) freshly dissolved in 50 mM sodium citrate buffer (pH 4.5) or citrate buffer as control for five consecutive days (referred to as multiple low-dose (MLD)-STZ). To create beta cell–specific *Mst1*$^{-/-}$ mice, mice harboring exon 4 of the *Mst1* gene flanked by *loxP* sites (*Mst1*$^{fl/fl}$)[55] were crossed with mice expressing Cre under the rat insulin-2 promoter (B6;D2-Tg(Ins-Cre)23Herr: RIP-Cre[63], provided by P. Herrera, University of Geneva and A. Mansouri, Max Planck Institute for Biophysical Chemistry). RIP-Cre-*Mst1*$^{fl/-}$ mice were intercrossed to generate RIP-Cre-*Mst1*$^{fl/fl}$. Mice were MLD-STZ injected as described above. For the high-fat diet (HFD) experiments, 8-week-old RIP-Cre-*Mst1*$^{fl/fl}$ (b*Mst1*$^{-/-}$) mice and their RIP-Cre littermates were fed a normal diet (ND, Harlan Teklad Rodent Diet 8604, containing 12.2, 57.6 and 30.2% calories from fat, carbohydrate and protein, respectively) or a high-fat, high-sucrose diet (HFD, Surwit Research Diets, New Brunswick, NJ, containing 58, 26 and 16% calories from fat, carbohydrate and protein, respectively[58,64]) for 20 weeks. For both models, random blood was obtained from the tail vein of nonfasted mice, and glucose was measured using a Glucometer (Freestyle; TheraSense, Alameda, CA). Mice were killed at the end of experiment, and pancreases were isolated. Throughout the whole study, food consumption and body weight were measured weekly. Only male mice were used in the experiments. All animals were housed in a temperature-controlled room with a 12-h light-dark cycle and were allowed free access to food and water in agreement with US National Institutes of Health animal care guidelines and the German animal protection law and approved by the Bremen Senate.

Intraperitoneal glucose and ITTs and measurement of insulin release. For i.p. GTTs, mice were fasted 12 h overnight and injected i.p. with glucose (40%; B. Braun, Melsungen, Germany) at a dose of 1 g per kg body weight. Blood samples were obtained at time points 0, 15, 30, 60, 90 and 120 min for glucose measurements using a glucometer and at time points 0, 15 and 30 min for measurement of serum insulin levels. For i.p. ITTs, mice were injected with 0.75 U per kg body weight recombinant human insulin (Novolin, Novo Nordisk) after a 5-h fast, and glucose concentration was determined with the glucometer. Insulin secretion was measured before (0 min) and after (15 and 30 min) i.p. injection of glucose (2 g per kg body weight) and measured using ultrasensitive mouse Elisa kit (ALPCO Diagnostics, Salem, NH).

Plasmids. pCMV-Myc-MST1 and kinase-dead pCMV-MST1-K59R (dn-MST1) was provided by J. Sadoshima and Y. Maejima (Rutgers New Jersey Medical School)[30]. Mouse pB.RSV.PDX1-GFP plasmid was provided by I. Leibiger (Karolinska University, Stockholm). pcDNA3 Myr-HA AKT1, pCDNA3 HA-ubiquitin and pCDNA3 Jnk1a1 (apf) (dn-JNK) plasmids were obtained from Addgene (Cambridge, MA). Mouse PDX1 mutants (T11, T126, T152, T155, T214 and T231) in the pCGIG5 vector were generated by site-directed mutagenesis as described previously[38]. All mutations were verified by sequencing. To make bacterial expression plasmids for PDX1 mutants, the complete mouse PDX1 coding sequence (WT and mutants) has been amplified by PCR using a specific set of primers from pCGIG5 plasmids and cloned into a pGEX-6P-1 bacterial expression vector (provided by R. Walther, University of Greifswald). The rat insulin–driven luciferase vector (RIP-luc) was constructed by subcloning a 700–base pair (bp) fragment containing 660 bp of the rat insulin-2 promoter (provided by R. Zinkernagel, University of Zurich) into a pMCS-Green-*Renilla*-Luc vector (Thermo Scientific). pCMV-Red Firefly Luc vector was obtained from Thermo Scientific.

Transfections. To knock down MST1 expression in human islets, SMARTpool technology from Dharmacon was used. A mix of ON-TARGETplus siRNAs directed against human MST1 sequences UAAAGAGACCGGCCAGAUU, GAUGGGCACUGUCCGAGUA, GCCCUCAUGUAGUCAAAUA and CCA GAGCUAUGGUCAGAUA and mouse Mst1 sequences GAUGGGCACUG UCCGAGUA, UGACAGCCCUCACGUAGUC, GCAGGUCAACUUACAG AUA and CUACAGCACCCGUUUGUUA. (100 nM, Dharmacon) was transiently transfected into human and mouse islets and efficiently reduced MST1 levels. An ON-TARGETplus nontargeting siRNA pool from Dharmacon served as a control. To knock down BIM and caspase-3 expression in human islets, siRNAs targeting human BIM (SignalSilence Bim SiRNA I, Cell Signaling) and caspase-3 (NEB) were used. GFP, MST1, dn-MST1 (K59R), dn-JNK1 and Myr-AKT1 plasmids were used to overexpress these proteins in human islets and INS-1E cells.

An adapted improved protocol to achieve silencing and overexpression in human islets was developed[19,65]. Islets were partially dispersed with accutase (PAA) to break islets into smaller cell aggregates to increase transfection efficiency and cultured on ECM dishes for at least 2 d. Isolated islets and INS-1E cells were exposed to transfection Ca^{2+}-KRH medium (KCl 4.74 mM, KH_2PO_4 1.19 mM, $MgCl_2$•$6H_2O$ 1.19 mM, NaCl 119 mM, $CaCl_2$ 2.54 mM, $NaHCO_3$ 25 mM and HEPES 10 mM). After 1-h incubation, lipoplexes (Lipofectamine 2000, Invitrogen)/siRNA ratio 1:20 pmol or –lipoplexes/DNA ratio 2.5:1) were added to transfect the islets and INS-1E cells. After an additional 6-h incubation, CMRL-1066 or RPMI-1640 medium containing 20% FCS and L-glutamine were added to the transfected islets or INS-1E cells. Efficient transfection was evaluated based on fluorescein-labeled siRNA (NEB) or eGFP-positive cells analyzed by fluorescent or confocal microscopy. HEK 293 cells were transiently transfected using Opti-MEM medium and Lipofectamine (Invitrogen) according to the manufacturer's instructions.

Glucose-stimulated insulin secretion. For acute insulin release in response to glucose, primary human and mouse islets and INS-1E cells were washed and preincubated (30 min) in Krebs-Ringer bicarbonate buffer (KRB) containing 2.8 mM glucose and 0.5% BSA. KRB was then replaced by KRB 2.8 mM glucose for 1 h (basal), followed by an additional 1 h in KRB 16.7 mM glucose with or without 100 nM GLP1 or 1 μM glibenclamide. Insulin content was extracted with 0.18N HCl in 70% ethanol. Insulin was determined using human and mouse insulin ELISA (ALPCO Diagnostics, Salem, NH). Secreted insulin was normalized to insulin content.

Immunohistochemistry. Pancreatic tissues were processed as previously described[66]. In brief, mouse pancreases were dissected and fixed in 4%

doi:10.1038/nm.3482

formaldehyde at 4 °C for 12 h before embedding in paraffin. Human and mouse 4-µm sections were deparaffinized, rehydrated and incubated overnight at 4 °C with anti-insulin (A0546, 1:50), anti-glucagon (A0565, 1:50) and rat anti–mouse Ki-67 (M7249, 1:50) antibodies from Dako, anti-pMST1 (3681, 1:100) and anti-Bim (2933, 1:100) antibodies from Cell Signaling Technology (CST), anti-PDX1 antibody (47267, 1:1,200) from Abcam and anti-Glut2 antibody (07-1402, 1:100) from Chemicon, followed by FITC- or Cy3-conjugated secondary antibodies (Jackson ImmunoResearch Laboratories, 1:100). Slides were mounted with Vectashield with DAPI (Vector Labs). For mouse sections or primary islets cultured on ECM dishes, beta cell apoptosis was analyzed by the TUNEL technique according to the manufacturer's instructions (*In situ* Cell Death Detection Kit, TMR red; Roche) and double stained for insulin. Fluorescence was analyzed using a Nikon MEA53200 (Nikon, Dusseldorf, Germany) microscope, and images were acquired using NIS-Elements software (Nikon).

Morphometric analysis. For morphometric data, ten sections (spanning the width of the pancreas) per mouse were analyzed. Pancreatic tissue area and insulin-positive area were determined by computer-assisted measurements using a Nikon MEA53200 (Nikon, Dusseldorf, Germany) microscope, and images were acquired using NIS-Elements software (Nikon). The number of islets (defined as insulin-positive aggregates at least 25 µm in diameter) was scored and used to calculate islet density (number of islets per square centimeter of tissue), mean islet size (the ratio of the total insulin-positive area to the total islet number on the sections). Mean percentage beta cell fraction per pancreas was calculated as the ratio of insulin-positive to whole pancreatic tissue area. Beta cell mass was obtained by multiplying the beta cell fraction by the weight of the pancreas. Morphometric beta cell and islet characterizations are results from analyses of at least 100 islets per mouse.

Western blot analysis. At the end of the incubation periods, islets and INS-1E cells were washed in ice-cold PBS and lysed in lysis buffer containing 20 mM Tris acetate, 0.27 M sucrose, 1 mM EDTA, 1 mM EGTA, 50 mM NaF, 1% Triton X-100, 5 mM sodium pyrophosphate and 10 mM β-glycerophosphate. Prior to use, the lysis buffer was supplemented with Protease and Phosphatase Inhibitors (Pierce, Rockford, IL, USA). Protein concentrations were determined with the BCA protein assay (Pierce). Equivalent amounts of protein from each treatment group were run on a NuPAGE 4–12% Bis-Tris gel (Invitrogen) and electrically transferred onto PVDF membranes. After 1-h blocking at room temperature using 5% milk (CST), membranes were incubated overnight at 4 °C with the following antibodies: rabbit anti-MST1 (3682), rabbit anti-pMST1 (3681), rabbit anti-ubiquitin (3933), rabbit anti-Bim (2933), rabbit anti-AKT (9272), rabbit anti-pAKT (Ser437) (4058), rabbit anti-Bax (2772), rabbit anti–Bcl-2 (2870), rabbit anti–Bcl-xL (2764), rabbit anti-Bad (9239), rabbit anti-pBad (5284), rabbit anti-PUMA (4976), rabbit anti-Bak (6947), rabbit anti-Mcl1 (4572), rabbit anti-pan–phosphorylated threonine (9381), mouse monoclonal anti-pan–phosphorylated threonine (9386), rabbit anti-pGSK-3 (9336), rabbit anti-pFOXO1 (9461), mouse anti-Myc (2276), rabbit anti–cleaved caspase-3 (9664), rabbit anti–cleaved caspase-9 (rat specific; 9507), rabbit anti–cleaved caspase-9 (human specific; 9505), rabbit anti–cytochrome *c* (4272), rabbit anti–cytochrome oxidase (4850), rabbit anti-pJNK (T183/Y185) (9251), rabbit anti–c-Jun (S63) (9261), rabbit anti-PARP (9542), rabbit anti-tubulin (2146), rabbit anti–glyceraldehyde 3-phosphate dehydrogenase (2118) and rabbit anti–β-actin (4967) all from CST); rabbit anti-pMST1 (79199), rabbit anti-GFP (290), mouse anti-NOXA (13654) and rabbit anti-PDX1 (47267) all from Abcam; rabbit anti-pH2B (07-191) from Millipore and rabbit anti-pPDX1 (T11) (PA5-13046) from Thermo Scientific, followed by horseradish-peroxidase–linked anti-rabbit or anti-mouse IgG (Jackson). All primary antibodies were used at 1:1,000 dilution in Tris-buffered saline plus Tween-20 (TBS-T) containing 5% BSA, except for the antibody to PDX1 (1:6,000). Membrane was developed using a chemiluminescence assay system (Pierce) and analyzed using DocITLS image acquisition 6.6a (UVP BioImaging Systems, Upland, CA, USA).

Immunoprecipitation. For immunoprecipitation, cells were washed with PBS and lysed in cold buffer containing 20 mM Tris-HCl (pH 7.5), 150 mM NaCl, 0.27 M sucrose, 1 mM EDTA, 1 mM EGTA, 50 mM NaF, 1% NP-40, 5 mM sodium pyrophosphate and 10 mM β-glycerophosphate supplemented with proteinase and phosphatase inhibitors for 30 min on ice. Lysates were centrifuged at 12,000*g* for 15 min at 4 °C before immunoprecipitation. Immunoprecipitations were carried out with incubating 0.5–1 mg of total lysate with rabbit anti-PDX1 (1:500; Abcam), rabbit anti-MST1 (1:50; CST), mouse anti-Myc (1:1,000; CST) and rabbit anti-GFP (1:1,000; Abcam) antibodies on a rotator at 4 °C overnight. Immunocomplexes were then captured with Protein A Agarose Fast Flow (Millipore) by rotation at 4 °C for 4 h. After five washes with cold lysis buffer, the immunoprecipitates were used for kinase assays or resuspended in sample buffer and separated by NuPAGE 4–12% Bis-Tris gels (Invitrogen).

***In vitro* kinase assay.** Purified human active MST1 without GST-tag (Upstate Biotechnology) or with GST-tag (Abcam) was incubated with ^{32}P-ATP (2 µCi, PerkinElmer Life Sciences), ATP (100 µM) and 1 mM dithiothreitol in a kinase buffer containing 40 mM HEPES (pH 7.4), 20 mM $MgCl_2$, 1 mM EDTA and 1 µg of purified recombinant human PDX1 (Abcam) or bacterially purified PDX1-GST (WT and mutants) as substrates. After incubation at 30 °C for 30 min, the reaction was stopped by adding loading buffer and proteins were separated on NuPAGE gels and phosphorylation levels visualized either by autoradiography or specific antibody for pPDX1 (T11) or pThr. The total PDX1 was detected with anti-PDX1 antibody.

***In vivo* kinase assay.** HEK 293 cells were transiently transfected with PDX1 and MST1 expression plasmids. Next, cell lysates were subjected to immunoprecipitation with anti-PDX1 antibody. The immunoprecipitates were separated by NuPAGE Bis-Tris gels and transferred to PVDF membranes and subsequently subjected to analyses of phosphorylation levels by pan–phosphorylated threonine antibody, which binds to threonine phosphorylated sites in a manner largely independent of the surrounding amino acid sequence or pan–phosphorylated serine antibody, which recognizes serine-phosphorylated proteins.

***In vivo* ubiquitination.** HEK 293 cells were cultured in 10-cm cell culture dishes and transfected with HA-ubiquitin and PDX1 and MST1 expression plasmids for 48 h. For ubiquitination in human islets, 5,000 islets per condition were transfected with ubiquitin plasmid. After 24 h, islets were infected with Ad-GFP or Ad-MST1 for 6 h and kept for another 48 h. HEK 293 cells and islets were exposed to 20 µM MG-132 for the last 6 h of the experiment. Lysates were immunoprecipitated with PDX1-specific antibody overnight at 4 °C. Immunocomplexes were then captured with Protein A Agarose by rotation at 4 °C for 4 h. After extensive washing, immunoprecipitates were boiled in sample buffer and proteins subjected to western blotting with ubiquitin-specific antibody.

Protein degradation analysis. HEK 293 cells were transfected with PDX1 alone or together with MST1 expression plasmids. Human islets were infected with Ad-GFP (control) or Ad-MST1. At 48 h after transfection or infection, cells were treated with 50 µg/ml translation initiation inhibitor CHX, which was added to the medium at the times indicated, and the lysates were subjected to western blotting.

RNA extraction and RT-PCR analysis. Total RNA was isolated from cultured human islets and INS-1E cells using TRIzol (Invitrogen), and RT-PCR was performed as described previously[67]. For analysis, we used the Applied Biosystems StepOne Real-Time PCR system (Applied Biosystems, CA, USA) with TaqMan(R) Fast Universal PCR Master Mix for TaqMan assays (Applied Biosystems). TaqMan(R) Gene Expression Assays were used for *PDX1* (Hs00426216_m1), *SLC2A2* (Hs01096905_m1), *GCK* (Hs01564555_m1), *INS* (Hs02741908_m1), *PPIA* (Hs99999904_m1), *BCL2L11* (Hs01083836_m1) and *TUBULIN* (Hs00362387_m1) for human and *Pdx1* (Rn00755591_m1), *Slc2a2* (Rn00563565_m1), *Gck* (Rn00688285_m1), *Ins1* (Rn02121433_g1), *Ins2* (Rn01774648_g1), *Ppia* (Rn00690933_m1) and *Tuba1a* (Rn01532518_g1) for rat.

Luciferase reporter assay. The transcriptional activity of the PDX1 at promoter level was evaluated using rat insulin-2–*Renilla* luciferase (Ins2–luc *Renilla*) reporter gene. HEK 293 cells were transfected with Ins2–luc *Renilla*,

pCMV-firefly, PDX1-WT or PDX1-T11A, alone or together with Myc-MST1 expression plasmids for 48 h. INS-1E cells transfected with Ins2-luc *Renilla* and pCMV-firefly plasmids and were infected with Ad-GFP or Ad-MST1 for 48 h. Luciferase activity was determined using the *Renilla* Firefly Luciferase Dual Assay Kit according to the manufacturer's instructions (Pierce). pCMV-firefly was used as transfection control.

Adenovirus infection. Isolated human islets and INS-1E cells were infected with adenovirus carrying eGFP as a control (provided by A.E. Karlsen, Novo Nordisk A/S, Denmark) or MST1 (Ad-MST1, provided by J. Sadoshima) at a multiplicity of infection (MOI) of 20 (for INS-1E) or 100 (for human islets) for 4 h. Adenovirus was subsequently washed off with PBS and replaced by fresh medium with 10% FBS, and GSIS or RNA and protein isolation performed after 48 or 72 h after infection.

Purification of PDX1-GST recombinant proteins. Expression and induction of recombinant GST proteins were performed as described previously[68]. *Escherichia coli* BL21 cells with various GST-fusion expression plasmids were cultured at 37 °C, and expression of recombinant proteins was induced by 0.1 mM final concentration of isopropyl-β-D-thiogalactoside (IPTG; Sigma) for 2.5 h. Cells were lysed using B-PER bacterial protein extraction reagent (Pierce) and purified using Glutathione Spin Columns (Pierce).

Cytochrome *c* release. Cytochrome *c* release was performed by digitonin-based subcellular fractionation technique[69]. Briefly, INS-1E cells were digitonin-permeabilized for 5 min on ice after resuspension of the cell pellet in 200 µl of cytosolic extraction buffer (250 mM sucrose, 70 mM KCl, 137 mM NaCl, 4.3 mM Na_2HPO_4 and 1.4 mM KH_2PO_4 (pH 7.2) with 300 µg/ml digitonin (Sigma). Cells were then centrifuged at 1,000*g* for 5 min at 4 °C. Supernatants (cytosolic fractions) were collected and pellets solubilized in the same volume of mitochondrial lysis buffer (50 mM Tris (pH 7.4), 150 mM NaCl, 2 mM EDTA, 2 mM EGTA, 0.2% Triton X-100 and 0.3% NP-40), followed by centrifugation at 10,000*g* for 10 min at 4 C. After centrifugation, supernatants, which are the heavy membrane fractions enriched for mitochondria, as well as cytosolic fractions were subjected to western blot analysis.

Generation of stably expressed shRNAMST1 INS1-E cell line. To knock down MST1 expression in INS-1E cells, two different lentiviral shRNA targeting MST1 or control shRNA vectors (pGIPZ collection, Open Biosystems, Huntsville, AL) were transfected into INS-1E cells, and stable clones were generated by selection with puromycin (1 to 2.5 µg/ml). Positive clonal cell lines were identified by immunoblotting using antibody directed against MST1. After selection, INS-1E lines were maintained in culture medium containing 1.5 µg/ml puromycin.

Statistical analyses. Samples were evaluated in a randomized manner by five investigators (A.A., V.K., S.K., T.Y. and Z.A.) who were blinded to the treatment conditions. To perform statistical analysis, at least 3 independent experiments from 3 different organ donors were performed for human islets, at least 3 independent experiments were performed for mouse islets and cell lines and at least 3 independent tissue samples or mice were included in the analyses, as reported in all figure legends. No statistical method was used to predetermine sample size. Data are presented as means ± s.e.m. Mean differences were determined by Student's *t*-tests. To account for multiplicity in the treated cells *in vitro* and in mice *in vivo*, a Bonferroni correction was used.

61. Schulthess, F.T. *et al.* CXCL10 impairs beta cell function and viability in diabetes through TLR4 signaling. *Cell Metab.* **9**, 125–139 (2009).
62. Maedler, K. *et al.* Distinct effects of saturated and monounsaturated fatty acids on beta-cell turnover and function. *Diabetes* **50**, 69–76 (2001).
63. Herrera, P.L. Adult insulin- and glucagon-producing cells differentiate from two independent cell lineages. *Development* **127**, 2317–2322 (2000).
64. Surwit, R.S., Kuhn, C.M., Cochrane, C., McCubbin, J.A. & Feinglos, M.N. Diet-induced type II diabetes in C57BL/6J mice. *Diabetes* **37**, 1163–1167 (1988).
65. Kang, H.C. & Bae, Y.H. Transfection of rat pancreatic islet tissue by polymeric gene vectors. *Diabetes Technol. Ther.* **11**, 443–449 (2009).
66. Shu, L. *et al.* Transcription factor 7-like 2 regulates beta-cell survival and function in human pancreatic islets. *Diabetes* **57**, 645–653 (2008).
67. Shu, L. *et al.* TCF7L2 promotes beta cell regeneration in human and mouse pancreas. *Diabetologia* **55**, 3296–3307 (2012).
68. Tolia, N.H. & Joshua-Tor, L. Strategies for protein coexpression in *Escherichia coli*. *Nat. Methods* **3**, 55–64 (2006).
69. Arnoult, D. Apoptosis-associated mitochondrial outer membrane permeabilization assays. *Methods* **44**, 229–234 (2008).

doi:10.1038/nm.3482